Deciphering metasomatic events beneath Mindszentkálla (Bakony-Balaton Highland Volcanic Field, western Pannonian Basin) revealed by single-lithology and composite upper mantle xenoliths

Levente Patkó[1,2,3]*, Zoltán Kovács[3,4]†, Nóra Liptai[1,2], László E. Aradi[3,5]‡, Márta Berkesi[1,2], Jakub Ciazela[6], Károly Hidas[7], Carlos J. Garrido[8], István J. Kovács[1,2] and Csaba Szabó[3]

[1]MTA FI Lendület Pannon LitH₂Oscope Research Group, Institute of Earth Physics and Space Science, Sopron, Hungary, [2]Institute of Earth Physics and Space Science, Eötvös Loránd Research Network, Sopron, Hungary, [3]Lithosphere Fluid Research Lab (LRG), Institute of Geography and Earth Sciences, Eötvös Loránd University, Budapest, Hungary, [4]Centre for Energy Research, Eötvös Loránd Research Network, Budapest, Hungary, [5]Department of Geosciences, University of Padua, Padua, Italy, [6]Institute of Geological Sciences, Polish Academy of Sciences, Wroclaw, Poland, [7]Departamento de Geología y Subsuelo, Centro Nacional Instituto Geológico y Minero de España del CSIC (CN IGME-CSIC), Project Office in Granada, Granada, Spain, [8]Instituto Andaluz de Ciencias de la Tierra, CSIC-UGR, Armilla, Spain

Single-lithology and composite xenoliths from Mindszentkálla (Bakony-Balaton Highland Volcanic Field) in the Carpathian-Pannonian region record geochemical evolution of the subcontinental lithospheric mantle. The dominant single-lithology xenoliths are orthopyroxene-rich (22 vol% on average) harzburgites. Three composite xenoliths contain either two or more domains including dunite, olivine-orthopyroxenite, orthopyroxenite, apatite-bearing websterite and amphibole-phlogopite-bearing vein. The presence of different lithologies is a result of at least two metasomatic events that affected the lithospheric mantle. The first event resulted in orthopyroxene enrichment thus formed harzburgitic mantle volumes (Group I xenoliths). Major- and trace element distributions of the bulk harzburgites differ from the geochemical trends expected in residues of mantle melting. In contrast, petrographic and geochemical attributes suggest that the harzburgite was formed by silica-rich melt - peridotitic wall rock interactions in a supra-subduction zone. Within the Group I xenoliths, two subgroups were identified based on the presence or lack of enrichment in U, Pb and Sr. Since these elements are fluid mobile, their enrichment in certain Group I xenoliths indicate reaction with a subduction-related fluid, subsequent to the harzburgite formation. The effect of a second event overprints the features of the Group I xenoliths and is evidenced in all domains of two composite xenoliths (Group II xenoliths). The general geochemical character involves enrichment of basaltic

major and minor elements (Fe, Mn, Ti, Ca) in the rock-forming minerals and convex-upward rare earth element (REE) patterns in clinopyroxenes. We suggest that the different domains represent reaction products with variably evolved basaltic melts of a single magmatic event. The tectonic background to the formation of Group I xenoliths is likely linked to the subduction of oceanic crust during the Mesozoic−Paleogene. This happened far from the current position of Mindszentkálla, to where the lithosphere, including the metasomatized mantle volume, was transferred *via* plate extrusion. The Group II xenoliths appear to bear the geochemical signature of a younger (Neogene) basaltic magmatic event, likely the same that produced the host basalt transporting the xenoliths to the surface.

1 Introduction

Mantle metasomatism is commonly understood as an interaction between melts/fluids varying from silicate to carbonate in composition and peridotitic or pyroxenitic wall- and host rocks (e.g., O'Reilly and Griffin, 2013 and references therein). Diverse conditions in different tectonic settings lead to variable metasomatic products in the mantle. In intraplate settings, the most common metasomatic agents are asthenosphere-derived basaltic melts, which dominantly cause olivine and clinopyroxene enrichment along melt migration paths (e.g., Shaw et al., 2018). If the basaltic melt reacts with refractory lithospheric mantle, the refertilization leads to a suite of compositions from lherzolites to websterites, on a wide range of observational scales (e.g., Garrido and Bodinier, 1999; Le Roux et al., 2007). In divergent settings, melting is a dominant process in the mantle. However, refertilization of the mantle is also possible further away from the melt channels (e.g., Hazra et al., 2021), since silica-undersaturated liquids such as olivine tholeiites along the ridges can crystallize both clinopyroxene and orthopyroxene (e.g., Green and Ringwood, 1967). In convergent tectonic environments, fluids released by the subducted slab can trigger partial melting in the mantle wedge (e.g, Iwamori, 1998; Grove et al., 2006). The intensive melt-rock reactions in the mantle wedge can modify the original composition of these melts, resulting in more evolved, silica-rich melts. During interactions between the silica-rich melts and the peridotites, wall rocks are usually enriched in orthopyroxene (e.g., Kelemen et al., 1992). The presence of small volumes of carbonated silicate melts in the mantle can be also linked to subduction (e.g., Yaxley et al., 2022), and often plays a role in the formation of wehrlitic compositions (e.g., Rudnick et al., 1993).

Upper mantle xenoliths being hosted by Neogene alkali basalts from the Carpathian–Pannonian region (CPR) have been extensively studied in the last decades, and metasomatic events related to different agents were identified. Dominantly, these events were either related to mafic melt migrations typical of intraplate settings, causing clinopyroxene enrichment (e.g., Liptai et al., 2017; Patkó et al., 2020), or silica-rich, more evolved melt infiltrations related to subduction environments which resulted in orthopyroxene-rich lithologies (e.g., Bali et al., 2007, 2008). The Bakony-Balaton Highland Volcanic Field (BBHVF), situated in the central part of the Pannonian Basin (Figure 1), is probably the most investigated xenolith-bearing volcanic field in the CPR, where several studies proposed mantle metasomatism by subduction-related melts/fluids (e.g., Embey-Isztin et al., 1989; Downes et al., 1992; Bali et al., 2002, 2007, 2008; Ntaflos et al., 2017). Despite the great number of research articles on the BBHVF mantle, the locality of Mindszentkálla was not investigated so far, except for two xenoliths (Créon et al., 2017b).

This study is focusing on 13 upper mantle xenoliths from Mindszentkálla, ten peridotites and three composites with both peridotitic and pyroxenitic domains. Our principal goals are to 1) decipher and characterize the metasomatic events that are responsible for the unusually heterogeneous lithology, and 2) constrain the possible links between the formation of different mantle domains and large-scale tectonic events affecting the lithospheric mantle of the study area.

2 Geological setting and sampling

The CPR is situated in East–Central Europe and includes the Pannonian Basin system framed by the Alpine, Carpathian and Dinaric orogenic belts (Figure 1A). The Pannonian Basin consists of two tectonic mega-units with different affinities referred to as ALCAPA in the northwest and Tisza-Dacia in the southeast (e.g., Csontos and Vörös, 2004), divided by the Mid-Hungarian shear zone (Csontos and Nagymarosy, 1998) (Figure 1A). The juxtaposition of the mega-units happened during the latest Oligocene to early Miocene after extrusion of the ALCAPA mega-unit (Kázmér and Kovács, 1985; Ratschbacher et al.,
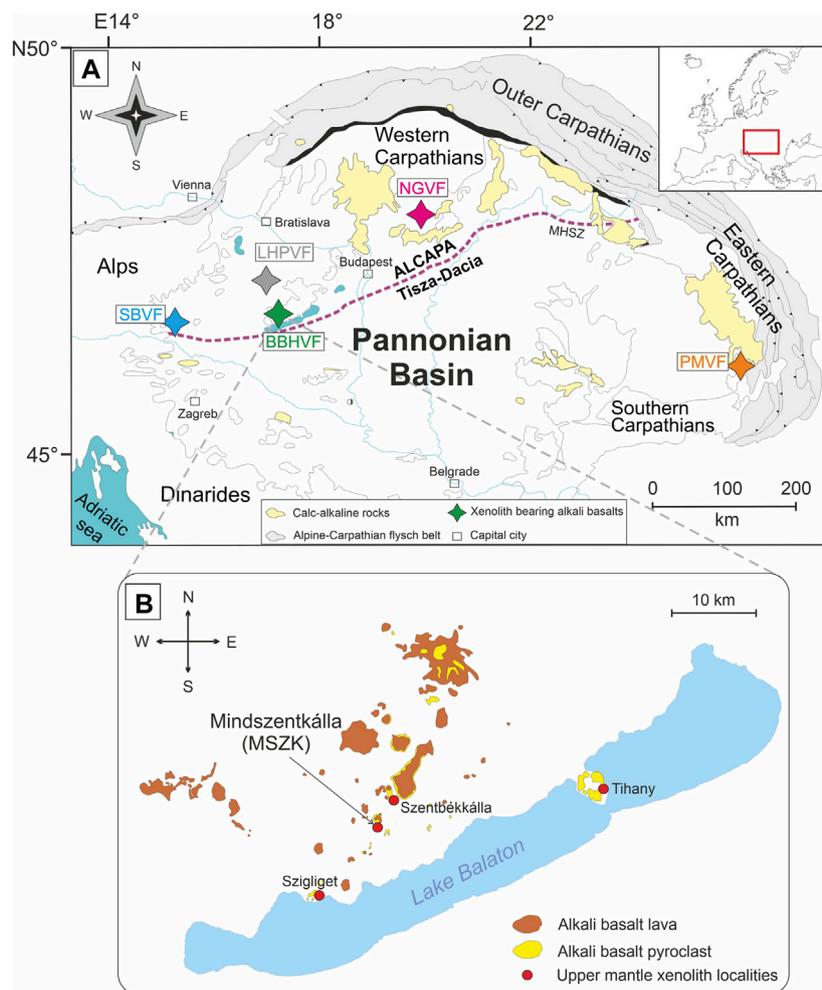
FIGURE 1
(A) Simplified geological map of the Carpathian-Pannonian region (CPR) with the boundary of the ALCAPA and Tisza-Dacia microplates, and the Mid-Hungarian shear zone (MHSZ) between them (Csontos and Nagymarosy, 1998 and references therein). Xenolith-bearing Neogene alkali basalt volcanic fields shown are the following: SBVF, Styrian Basin Volcanic Field; LHPVF, Little Hungarian Plain Volcanic Field; BBHVF, Bakony-Balaton Highland Volcanic Field; NGVF, Nógrád-Gömör Volcanic Field; PMVF, Persani Mountains Volcanic Field. **(B)** Mindszentkálla xenolith locality together with other xenolith-bearing sites (Szigliget, Szentbákkálla, Tihany) in the Bakony-Balaton Highland Volcanic Field (modified after Hidas et al., 2010 and references therein).

1991) due to the northward movement of the Adriatic microplate and slab rollback (e.g., Fodor et al., 1999). During the middle Miocene, large-scale extension dominated the region leading to significant thinning of the lithosphere and updoming of the asthenosphere (Horváth, 1993). Several theories were proposed for what process induced the extension: subduction roll-back (Royden et al., 1982), thermal erosion related to the asthenospheric doming (Stegena et al., 1975), gravitational instability of the mantle lithosphere (Houseman and Gemmer, 2007), or various combinations combination of these. Following this stage, the collision of ALCAPA and Tisza-Dacia with the stable European platform gradually led to a compressive phase starting in the late Miocene (Horváth and Cloetingh, 1996).

During the Neogene, widespread volcanism took place in the CPR including silicic, calc-alkaline and alkali volcanic products (e.g., Szabó et al., 1992; Seghedi and Downes, 2011). The study area of BBHVF (Figure 1B) is a monogenetic alkali basaltic province (Németh and Martin, 1999). The formation of alkali basalts can be attributed to extension-related adiabatic decompression melting of the upwelling asthenosphere (e.g., Embey-Isztin et al., 1993). Alternatively, compression appearing in the tectonic inversion stage (<8 Ma) of the evolution of the CPR may have squeezed partial melts from the hydrated asthenospheric dome (Kovács et al., 2020). The BBHVF comprises ~100 alkali basaltic volcanic centers including scoria cones, tuff rings, maar volcanic complexes and shield

TABLE 1 Petrographic properties and calculated equilibration temperatures of the studied xenoliths. Equilibration temperatures were calculated using thermometers as follows: T_{BK}, two-pyroxene method of Brey and Köhler (1990); T_{NG}, Ca-in-opx method of Brey and Köhler (1990) modified by Nimis and Grütter (2010); T_{WES}, Al and Cr in opx method of Witt-Eickschen and Seck (1991); T_{REE}, REE method of Liang et al. (2013). Abbreviations: ol—olivine; opx—orthopyroxene; cpx—clinopyroxene; sp—spinel; amp—amphibole; phl—phlogopite; ap—apatite; mp—melt pocket; ol-orthopyroxenite - olivine-orthopyroxenite.

Xenolith	Lithology	Texture	Modal composition (vol%)								Group	Equilibration temperature (˚C)			
			ol	opx	cpx	sp	amp	phl	ap	mp		T_{BK}	T_{NG}	T_{WES}	T_{REE}
MSZK0701	harzburgite	equigranular	68	27.5	4	0.5	—	—	—	—	IA	876	897	880	1,070 ± 29
MSZK0702	harzburgite	equigranular	73	19	3	1	0.5	—	—	3.5	IB	899	902	870	1,023 ± 27
MSZK1301A	harzburgite	coarse granular	85	12	3	trace	—	—	—	—	IA	1,008	986	961	1,052 ± 7
MSZK1301B	harzburgite	coarse granular	75.5	19.5	4	1	—	—	—	—	IA	992	986	964	1,082 ± 34
MSZK1301C	harzburgite	coarse granular	80.5	13.5	4.5	1	—	—	—	—	IB	1,017	1,016	997	1,077 ± 22
MSZK1302	harzburgite	equigranular	42	52	5	1	—	—	—	—	IB	769	903	879	1,084 ± 5
MSZK1307	harzburgite	equigranular	72.5	17.5	1	0.5	1	—	—	7	IB	890	911	874	979 ± 10
MSZK1309	harzburgite	equigranular	80	17	3	0.5	—	—	—	—	IB	804	904	872	1,097 ± 25
MSZK1310	harzburgite	equigranular	71	24.5	1	3.5	—	—	—	—	IA	831	900	883	1,053 ± 9
MSZK1311	harzburgite	equigranular	78	17.5	3.5	1	—	—	—	—	IB	856	899	883	1,053 ± 10
MSZK1301D	dunite	coarse granular	99	trace	trace	0.5	—	—	—	—	IA	814	898	854	1,079 ± 5
	ol-orthopyroxenite	equigranular	17.5	79.5	3	trace	—	—	—	—	IB	853	899	878	1,046 ± 15
MSZK1305	harzburgite	equigranular	78.5	18	3	0.5	—	—	—	—	II	885	929	835	1,061 ± 12
	orthopyroxenite	equigranular	—	96	3	0.5	—	—	—	0.5	II	882	939	832	1,032 ± 12
	websterite	magmatic	—	30	70	—	—	—	trace	—	II	938	1,004	720	1,154 ± 31
	[amp-phl vein]	magmatic	—	—	—	—	70	20	—	10	II	—	—	—	—
MSZK1306B	harzburgite	equigranular	70	26.5	3	0.5	—	—	—	—	II	874	928	871	1,056 ± 8
	orthopyroxenite	equigranular	—	98	—	1.5	—	—	—	0.5	II	—	956	766	—
	websterite	magmatic	—	29.5	70	trace	trace	—	0.5	—	II	858	1,043	721	1,123 ± 8

volcanoes (Németh and Martin, 1999). The volcanism took place between 8–2 Ma, evidenced by both K-Ar (Balogh and Németh, 2005; Pécskay et al., 2006) and $^{40}Ar/^{39}Ar$ geochronology (Wijbrans et al., 2007). The eruptive centers are often characterized by extensive feeding systems with complex evolution history (Jankovics et al., 2019).

In the BBHVF, the alkali basaltic volcanic activity brought numerous lower crustal (Török et al., 2014) and upper mantle xenoliths (Szabó et al., 2004) to the surface at 9 and 6 outcrops, respectively. Upper mantle xenoliths with depleted geochemical features are subordinate among the BBHVF xenoliths, but were thoroughly studied (Embey-Isztin et al., 1989; Downes et al., 1992). In contrast, mantle xenoliths from this region are abundantly metasomatized, formed by the reaction between melts and/or fluids. The metasomatizing fluids are dominated by CO_2, but H_2O, dissolved silicate melt component and S-bearing volatile phases were also detected in fluid inclusions (e.g., Hidas et al., 2010; Berkesi et al., 2012; Créon et al., 2017a). In the BBHVF, both carbonate (Bali et al., 2002; Demény et al., 2004) and silicate melts were revealed, the latter often with silica-rich compositions (Bali et al., 2007, 2008; Créon et al., 2017b; Németh et al., 2021). These suggest that crustal components

played a key role in the evolution of the upper mantle beneath the study area.

The Mindszentkálla (MSZK) locality covers three sampling sites (Supplementary Figure S1) situated on the slopes of Kopasz Hill, ~1 km to the west of Mindszentkálla village. Kopasz Hill is a vent complex that is one of the youngest (2.8–2.5 Ma) volcanic erosion remnants in the BBHVF (Kereszturi and Németh, 2011). Eighteen upper mantle xenoliths were collected at the MSZK locality, out of which 13 (Table 1) were selected for detailed petrographic and geochemical analyses. These selected tuff-hosted xenoliths have angular shapes and a size range of 4–7 cm in diameter. There is no macroscopic evidence of interaction between the host basalt and the xenoliths. The studied xenoliths are fresh and exhibit no sign of weathering.

3 Analytical techniques

Petrographic examination of the xenoliths was conducted with a Nikon Eclipse LV100 POL polarizing microscope at the Lithosphere Fluid Research Laboratory (LRG), and with an AMRAY 1830 I/T6 scanning electron microscope at the

Department of Petrology and Geochemistry at Eötvös Loránd University (Budapest). The modal compositions were determined by applying a point counting method using the JMicroVision software (Roduit, 2006), counting at least 500 points per xenolith or 300 points per lithological domain in composite xenoliths.

The *in situ* major element analyses of the rock-forming minerals were determined using a CAMECA SX100 probe at the Dionýz Štúr State Geological Institute, Bratislava (Slovakia) with an accelerating voltage of 15 kV and a sample current of 20 nA. Beam diameter of 3–10 μm was used in dependence of available space for analysis and type of mineral: for silicates containing alkalis such as Na and K (amphibole, phlogopite) a larger (e.g., 10 μm), whereas for anhydrous, more stable and beam-resistant minerals (olivine, pyroxenes, spinel) a smaller beam size was applied (e.g., 3–5 μm). Counting times were 10–30 s to improve counting statistics. The detection limits of measured elements range from 0.02 to 0.05 wt%, and inaccuracies from 0.02 to 0.05 wt% (1σ), depending on the concentration. Raw X-ray counts were recalculated to weight percentages using the PAP correction program (Pouchou and Pichoir, 1991).

In situ trace element analyses of clinopyroxenes, orthopyroxenes, amphiboles, phlogopites and apatites were determined by laser ablation inductively coupled plasma mass spectrometry (LA-ICP-MS) at the Instituto Andaluz de Ciencias de la Tierra (IACT) in Armilla (Granada, Spain). This method covers the combination of Photon Machines Excimer (Analyte Excite) Laser technic attached to an Agilent 8800 QQQ based inductively coupled plasma mass spectrometer. The laser acquisition parameters were: 193 nm wavelength, ~12 J/cm^2 energy density, 10 Hz repetition rate and 40–110 μm spot size. After 30 s gas background analyses, samples were ablated for 60 s. The calibration standard was the NIST612 synthetic glass (Pearce et al., 1997). The internal standard was the ^{28}Si isotope for orthopyroxene, amphibole and phlogopite and the ^{44}Ca isotope for clinopyroxene and apatite. For quality control BIR-1G Glass (Jochum et al., 2005) was applied as a secondary standard. Data processing was carried out using the Iolite 2.5 software (Paton et al., 2011).

4 Petrography

The studied xenoliths have peridotitic (dunite, harzburgite) and pyroxenitic (olivine-orthopyroxenite, orthopyroxenite, websterite) lithologies (Figure 2). Most of the xenoliths exhibit one lithology type (harzburgite), however, three xenoliths are composites. The MSZK1301D composite xenolith has domains of dunite (I. on Figure 3A) and olivine-orthopyroxenite (II. on Figure 3A); the MSZK1306B is composed of harzburgite, orthopyroxenite and websterite (I., II. and III. on Figure 3B, respectively); whereas the xenolith MSZK1305 is built up by

FIGURE 2
Modal composition of the studied BBHVF xenoliths on Streckeisen (1976) diagram, along with xenolith data from previous studies in the area (Embey-Isztin et al., 1989; Downes et al., 1992; Török and De Vivo, 1995; Bali et al., 2002, 2007; Falus et al., 2004; Hidas et al., 2007; 2010; Nédli et al., 2009; Berkesi et al., 2012; Ntaflos et al., 2017; Liptai et al., 2021) and the average composition of the European subcontinental lithospheric mantle (SCLM; Downes, 1997) indicated with a dashed line. Abbreviations: ol - olivine; opx - orthopyroxene; cpx - clinopyroxene.

harzburgite, orthopyroxenite, websterite and amphibole-phlogopite vein (I., II., III. and IV. on Figure 3C, respectively). The orthopyroxenite domains are situated between the websterite and harzburgite parts in the composite xenoliths (Figures 3B,C). The contact zone between the websterite and orthopyroxenite domains is irregular and characterized by eroded orthopyroxenes and numerous melt pockets with the size of 200–500 μm in the orthopyroxenite domain (Figure 3D). In contrast, the contact is sharp between both the dunite and olivine-orthopyroxenite and the orthopyroxenite and harzburgite domains. The orthopyroxenes of the orthopyroxenite domains occasionally reflect growth at the expense of olivines of the neighboring harzburgite domains in their contact zone (Figures 3B,C). However, this phenomenon was not observed between the olivine-orthopyroxenite and dunite domains. The amphibole-phlogopite vein crosscuts the orthopyroxenite domain in xenolith.

MSZK1305 (Figure 3C) and is accompanied by eroded orthopyroxene grains, newly-formed clinopyroxenes with orthopyroxene remnants in their core, and melt pockets (Figure 3E).

In the single-lithology harzburgites, olivine and orthopyroxene abundances vary between 68–85 and 12–27.5 vol%, respectively (Table 1). The only exception is xenolith MSZK1302, which has lower olivine (42 vol%) and higher orthopyroxene (52 vol%) content. Clinopyroxene and
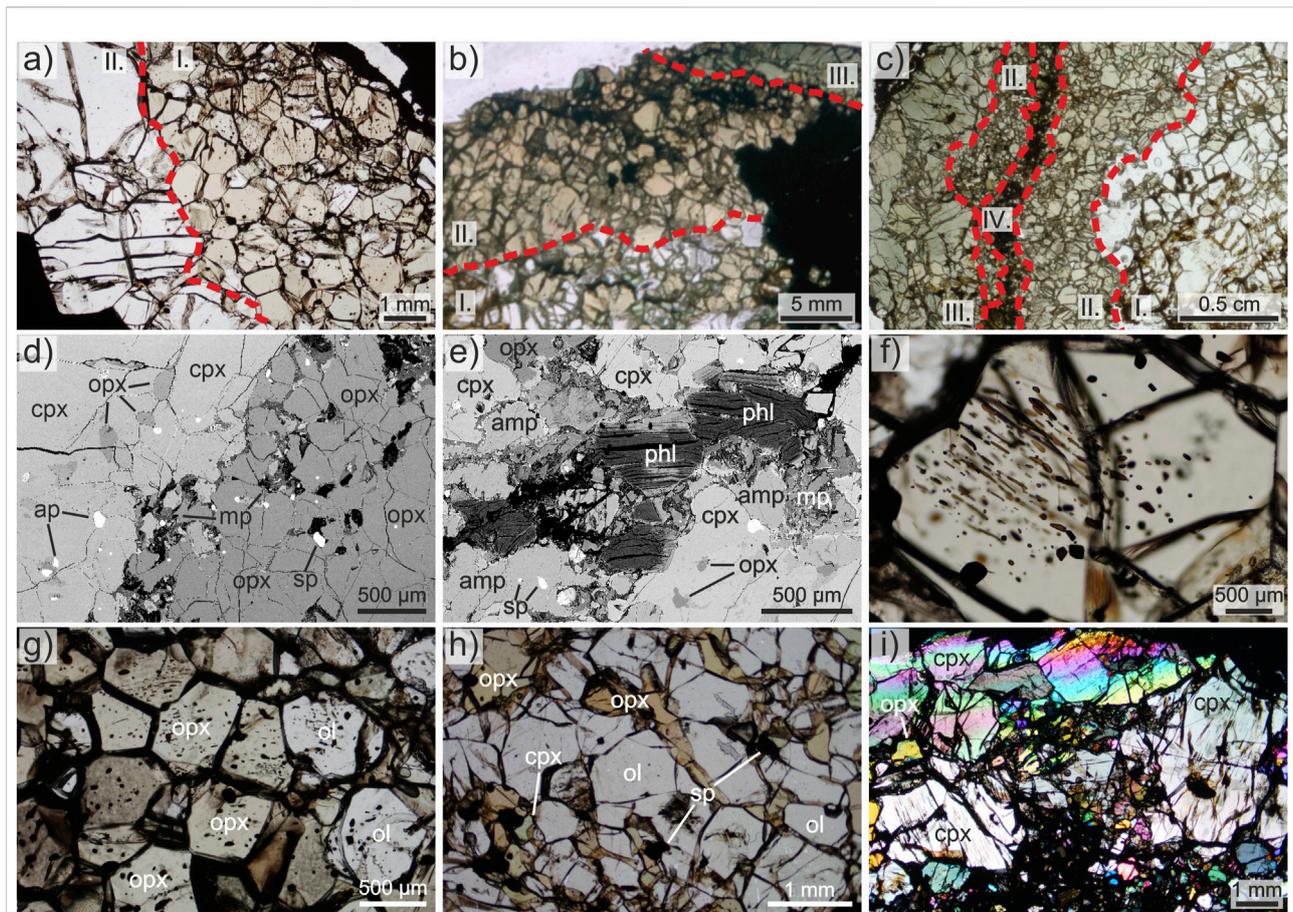
FIGURE 3
Photomicrographs of upper mantle xenoliths from Mindszentkálla (Bakony-Balaton Highland Volcanic Field) showing different textural characteristics. **(A)** Composite xenolith with olivine-orthopyroxenite (I) and dunite (II) domains (transmitted, plane-polarized light) (MSZK1301D). **(B)** Composite xenolith with harzburgite (I), orthopyroxenite (II) and websterite (III) domains (scanned image) (MSZK1306B). **(C)** Composite xenolith with harzburgite (I), orthopyroxenite (II) websterite (III) and amphibole-phlogopite vein (IV) domains (scanned image) (MSZK1305). **(D)** Contact zone between orthopyroxenite (right side) and websterite domains (left side) with resorbed orthopyroxenes in the former in a composite xenolith (backscattered electron image) (MSZK1306B). **(E)** Detailed image of the amphibole-phlogopite vein (backscattered electron image) (MSZK1305). **(F)** Numerous spinel inclusions hosted in orthopyroxene in a harzburgite (transmitted, plane-polarized light) (MSZK0701). **(G)** Equigranular textured harzburgite (transmitted, plane-polarized light) (MSZK1302). **(H)** Coarse granular textured harzburgite (transmitted, plane-polarized light) (MSZK1301B). **(I)** Magmatic textured websterite in the upper part of the photo (transmitted, cross-polarized light) (MSZK1305). Abbreviations: ol–olivine; opx–orthopyroxene; cpx–clinopyroxene; sp–spinel; amp–amphibole; phl–phlogopite; ap–apatite; mp–melt pocket.

spinel are minor constituents in these xenoliths with <5 and <4 vol% modal proportion, respectively. The silicates, especially the orthopyroxenes contain dozens of small (10–50 µm) elongated and rounded spinel inclusions in certain harzburgites (MSZK0701, MSZK1302, MSZK1309, MSZK1311) (Figures 3F,G). In two harzburgite xenoliths (MSZK0702, MSZK1307), traces of amphibole (0.5 and 1 vol%, respectively) were also observed in the core of 300–500 µm-sized melt pockets composed of secondary olivine, clinopyroxene, spinel and glass (Supplementary Figure S2A). The harzburgitic domains of the composite xenoliths show modal compositions similar to the single harzburgite xenoliths (Table1). Harzburgites have dominantly equigranular (75%) and less frequently coarse granular (25%) textures. In the

equigranular texture (Mercier and Nicolas, 1975), the subhedral grains meet in 120° triple points and the prevalent grain size is ~500 µm in diameter (Figure 3G). The coarse granular texture (Lenoir et al., 2000) is characterized by larger subhedral olivines (~1,000 µm) and smaller elongated pyroxenes (~1,000 µm long and ~300 µm wide) (Figure 3H).

In the coarse granular dunite domain (Figure 3A), pyroxenes and spinel only appear as accessories (<1 vol%) (Table 1). The olivine-orthopyroxenite domain contains some olivine (17.5 vol %), whereas it is completely absent in the orthopyroxenite domains. The traces of the pyroxenes occur as small (40–60 µm) inclusions within large olivines (>500 µm) in the dunite domain (Supplementary Figure S2B). In the olivine-orthopyroxenite domain the orthopyroxenes and the olivines

host numerous tiny (10–50 μm) rounded and elongated spinel inclusions (Figures 3F,G). Both in the olivine-orthopyroxenite and the orthopyroxenite domains, which have equigranular texture (Figure 3G), clinopyroxene (except for the orthopyroxenite domain in xenolith MSZK1306B) and spinel are trace constituents (≤3 vol%).

Both websterite domains contain ~30 vol% orthopyroxene and 70 vol% clinopyroxene. Interstitial and clinopyroxene-hosted, 10–80 μm-sized traces of apatite grains (≤0.5 vol%) also appear in the websterite domains (Figure 3D). The websterite domains have magmatic texture (Pike and Schwarzman, 1977) with large (3,000–5,000 μm), tabular clinopyroxene and smaller (500–800 μm) interstitial orthopyroxene grains (Figure 3I).

The amphibole-phlogopite vein is dominated by amphibole (70 vol%). The size of the frequently euhedral amphibole and phlogopite grains ranges between 200–600 μm (Figure 3E) and they show magmatic texture.

5 Geochemistry

5.1 Major elements of minerals

Based on the major element geochemistry of the rock-forming minerals, two groups (Group I and II) can be distinguished within the MSZK xenolith series. Group I consists of the single-lithology harzburgite xenoliths and the dunite and olivine-orthopyroxenite domains of the composite xenolith MSZK1301D (Table 1). Group II includes all domains (harzburgite, orthopyroxenite, websterite, amphibole-phlogopite vein) of two, multiple composite xenoliths (MSZK1305; MSZK1306B) (Table 1).

The Mg# (=Mg/[Mg+Fe^{2+}] of olivines in Group I xenoliths have a narrow range (0.90–0.91) (Figure 4A; Supplementary Figures S3A,B; Supplementary Table S1) corresponding to the average value characteristic for Phanerozoic mantle (Gaul et al., 2000). In contrast, olivines in the harzburgitic domains of Group II xenoliths have lower Mg# values (0.87; Supplementary Figures S3A,B). Group I xenoliths have lower MnO (0.13–0.15 wt%) and NiO (0.39–0.41 wt%) concentrations in olivine compared to those in the harzburgitic domains of Group II xenoliths (0.20 and 0.42–0.47 wt%, respectively) (Supplementary Figures S3A,B).

Orthopyroxenes of Group I xenoliths have narrow compositional ranges (Mg#: 0.90–0.91; Cr$_2$O$_3$: 0.36–0.66 wt%; CaO: 0.58–0.90 wt%) (Figures 4B,C; Supplementary Table S2). In contrast, in Group II xenoliths they have lower Mg# and Cr$_2$O$_3$, and variable CaO contents (Figures 4B,C). In the orthopyroxenes of Group II lithologies, Mg# and Cr$_2$O$_3$ is decreasing and CaO is increasing from the harzburgites through orthopyroxenites to websterites. (Figures 4B,C). The Al$_2$O$_3$ and SiO$_2$ concentrations are higher in Group I xenoliths (1.76–3.07, 55.0–57.4 wt%,

respectively) than in the Group II xenoliths (1.23–1.97, 53.3–56.1 wt%, respectively) (Supplementary Figure S3C). Contrarily, TiO$_2$ and MnO contents are slightly elevated in the Group II (0.05–0.20, 0.21–0.42 wt%, respectively) with respect to Group I xenoliths (0.01–0.10, 0.14–0.19 wt%, respectively) (Supplementary Figure S3D).

In Group I xenoliths, clinopyroxenes have similar Mg# (0.91–0.94), SiO$_2$ (52.2–54.2 wt%) TiO$_2$ (0.02–0.25 wt%) to those in the harzburgitic domains of Group II xenoliths (0.91, 53.0–53.6, 0.13 wt%, respectively) (Figures 4D,E; Supplementary Table S3). In contrast, clinopyroxenes in the orthopyroxenite and websterite domains have lower Mg# (0.80–0.89) and higher TiO$_2$ (0.33–0.55 wt%) contents (Figures 4D,E). The Al$_2$O$_3$, CaO and Na$_2$O concentrations in the clinopyroxenes show no systematic variations between the different xenolith groups.

The Cr# (=Cr/[Cr+Al]) of spinels has a partially overlapping range between Group I (0.35–0.53) and the Group II xenoliths (0.44–0.62) (Figure 4A) (Supplementary Table S4). Spinel Mg# (0.65–0.71) and MnO (0.24–0.32 wt%) in Group I xenoliths are higher than in Group II xenoliths (0.21–0.59 and 0.33–0.42 wt%, respectively) (Supplementary Figure S3E). Spinel in the websterite domain of composite xenolith MSZK1306B is extremely rich in TiO$_2$ (53.2 wt%), classifying it as ulvöspinel.

The amphiboles are pargasites in the harzburgite and the amphibole-phlogopite vein and Ti-rich pargasites in the websterite domain (Hawthorne et al., 2012; Supplementary Table S5). Amphiboles in Group I harzburgite xenoliths have higher Mg# (0.90), Cr$_2$O$_3$ (2.13–2.22 wt%) and lower TiO$_2$ (0.27–0.43 wt%), MnO (0.06 wt%) and K$_2$O (0.28–0.52 wt%) contents compared to those in Group II xenoliths (0.79–0.85, 0.14–0.52, 2.66–2.89, 0.08–0.12, 0.83–1.31 wt%, respectively) (Supplementary Figures S3F–H).

Micas only occur in a Group II composite xenolith (MSZK1305), and they are phlogopites based on their major element composition (Supplementary Table S6). Their Mg# shows a moderate range (0.86–0.89) and correlates positively with Al$_2$O$_3$ and negatively with the Cl content (Supplementary Figures S3I,J).

Apatites, which occur only in the websterite domain of Group II composite xenoliths (MSZK1305; MSZK1306B), are rich in F (>0.9 wt%) and Cl (>0.9 wt%) (Supplementary Table S7).

5.2 Trace elements of minerals

Trace element compositions of the MSZK xenoliths are variable, and support the distinction between the Group I and II xenoliths, as well as allowing the subdivision of Group I xenoliths.

Trace element compositions of orthopyroxenes are listed in Supplementary Table S8. The orthopyroxenes of Group I xenoliths show positive Pb and Ti anomalies (Figures 5A,B).
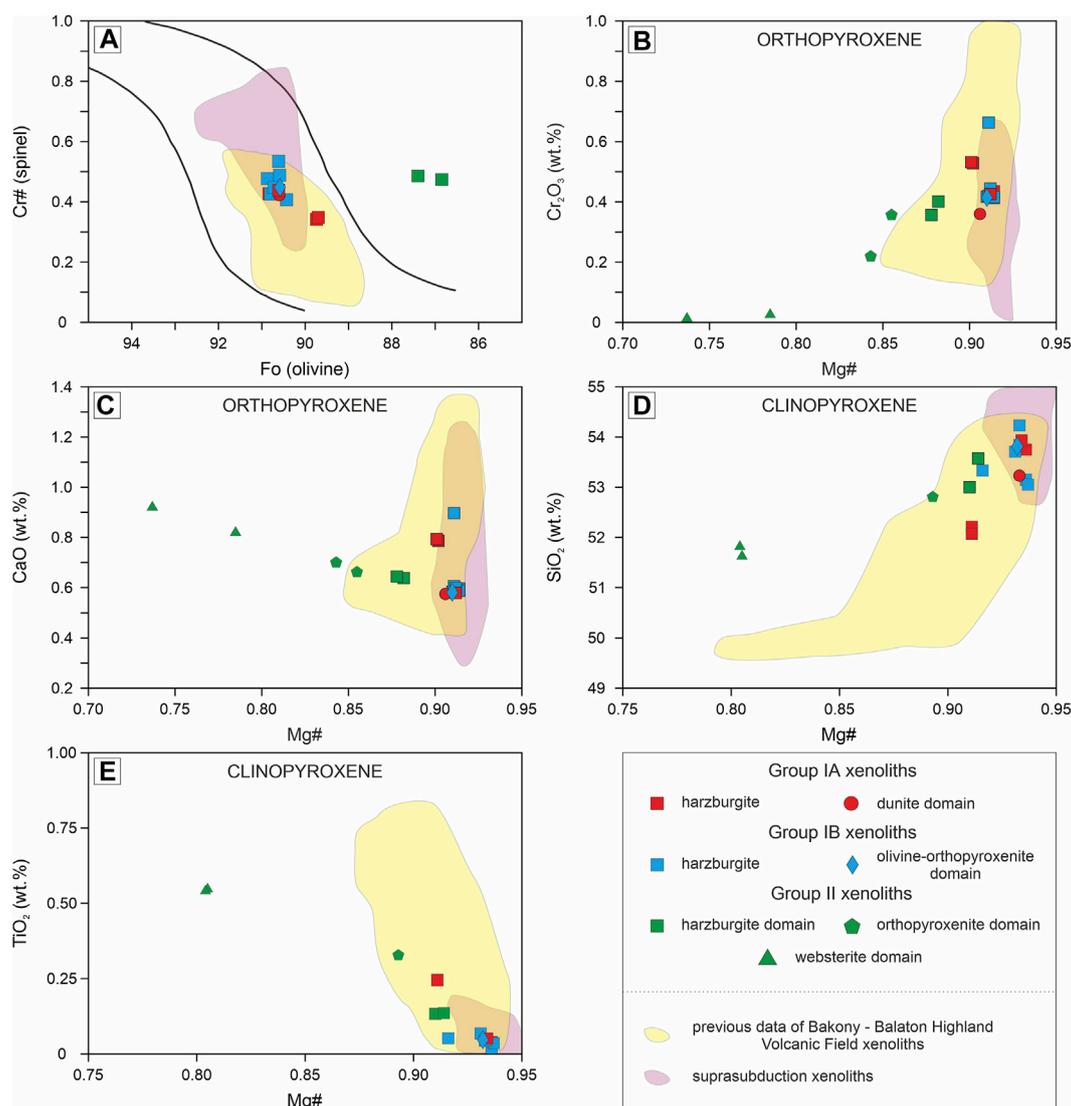
FIGURE 4
Major element composition of the studied MSZK xenoliths. **(A)** OSMA (olivine-spinel mantle array; Arai, 1994, indicated by solid lines); **(B)** variation of Mg# vs. Cr$_2$O$_3$ in orthopyroxene; **(C)** variation of Mg# vs. CaO in orthopyroxene; **(D)** variation of Mg# vs. SiO$_2$ in clinopyroxene; **(E)** variation of Mg# vs. TiO$_2$ in clinopyroxene. Published BBHVF upper mantle xenoliths: Embey-Isztin et al., 1989; 2001; 2014; Downes et al., 1992; Bali et al., 2002; 2007; 2018; Dobosi et al., 2003; 2010; Demény et al., 2004; Hidas et al., 2007; 2010; Berkesi et al., 2012; Ntaflos et al., 2017; Créon et al., 2017b. Data of supra-subduction xenoliths: McInnes et al., 2001; Ishimaru et al., 2007; Aradi et al., 2020. Mg#=Mg/[Mg+Fe^{2+}]; Fo refers to the forsterite content of olivine; Cr#=Cr/[Cr+Al].

In some xenoliths (Figure 5B), U positive anomalies are also seen. The primitive mantle (PM)-normalized (McDonough and Sun, 1995) REY (REE+Y) patterns of orthopyroxenes in Group I xenoliths show homogeneous distribution with increasing values from La to Lu (Figures 5D,E). In Group II xenoliths, all lithologies show similar trace element contents except for Cr that indicates depletion in the websterite domain (Figure 5C). The PM-normalized REY patterns of Group II xenoliths are characterized by gradual increase from La to Sm, followed by a flat distribution from Sm to Lu (Figure 5F).

Clinopyroxenes in Group I xenoliths show low trace element contents (Supplementary Table S9) compared to the PM (Figures 6A,B). The normalized value for high field strength elements (HFSE) such as Nb, Ta, Hf, Zr or Ti are low, never exceeding the PM value (Figures 6A,B). In contrast, there is a significant enrichment in U, Pb and Sr with respect to their neighboring elements in some xenoliths classified as Group IB (Figure 6B). This is not the case for the other part of Group I xenoliths, defining Group IA subgroup (Figure 6A). The REY distributions are similar in Group IA and IB xenoliths with enriched and flat patterns characteristic in both groups. Except for
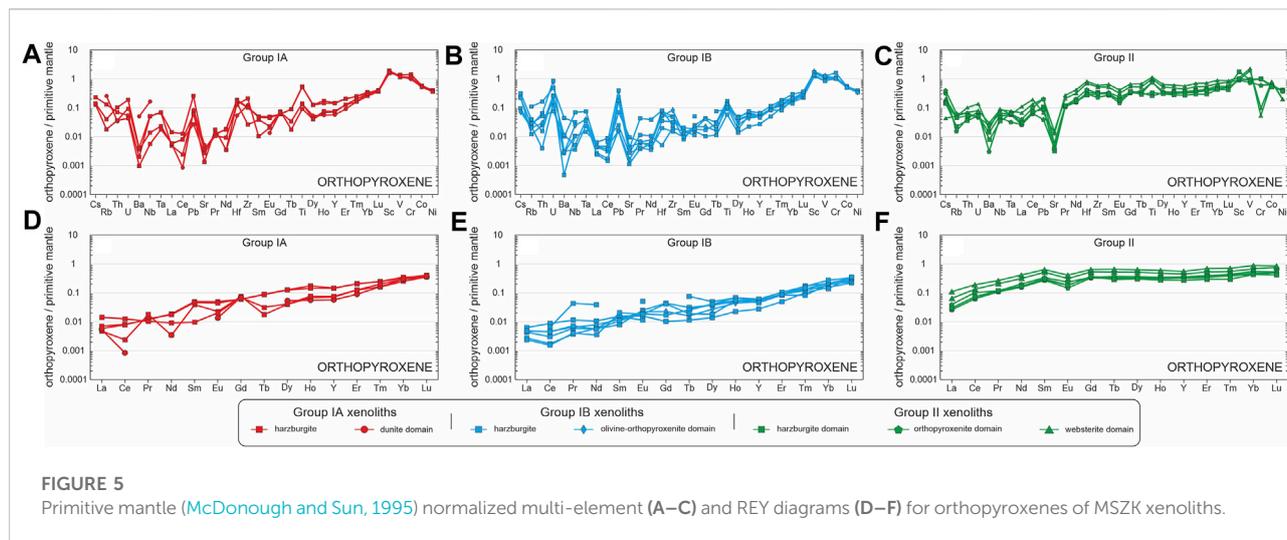
FIGURE 5
Primitive mantle (McDonough and Sun, 1995) normalized multi-element **(A–C)** and REY diagrams **(D–F)** for orthopyroxenes of MSZK xenoliths.
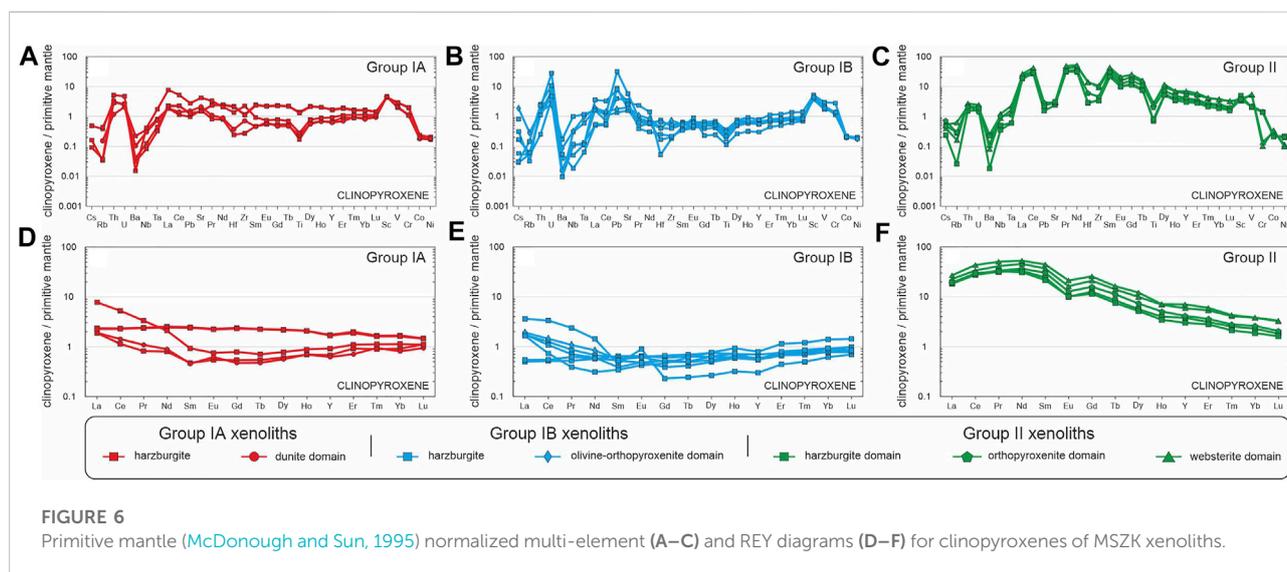
FIGURE 6
Primitive mantle (McDonough and Sun, 1995) normalized multi-element **(A–C)** and REY diagrams **(D–F)** for clinopyroxenes of MSZK xenoliths.

two Group IA (MSZK1301A; MSZK1301B) and one Group IB (MSZK1311) xenoliths, clinopyroxenes in Group I xenoliths show U-shaped patterns (synchronous $(La/Sm)_N$ >1 and $(Sm/Lu)_N$ < 1, where N denotes normalization to the PM of McDonough and Sun (1995)) (Figures 6D,E; Supplementary Table S9). In a Group IB harzburgite (MSZK1309), a positive Eu anomaly is observed (Figure 6E). The clinopyroxenes of Group II xenoliths have uniform trace element distribution independent of their lithology, except for V and Cr, which are enriched and depleted, respectively, in websterites compared to other lithologies (Figure 6C). Group II clinopyroxenes have higher HFSE and REY concentrations with respect to those in Group IA and IB xenoliths (Figure 6), and show depressions at Pb-Sr (Figure 6C). All Group II xenoliths show convex-upward REY patterns with negative Eu anomalies (Figure 6F).

Amphiboles in Group II xenoliths have higher trace element concentrations compared to those in Group IB harzburgites, which in contrast show well-defined positive U, Pb and Sr anomalies (Supplementary Table S10; Figure 7A). The REY patterns of amphiboles in the Group IB harzburgites are flat with minor enrichment in La and Ce in xenolith MSZK1307 (Figure 7D). Enrichment of light rare earth elements (LREE) is articulated in the websterite domain of composite xenolith MSZK1306B (Figure 7D). The amphiboles in the amphibole-phlogopite vein show convex-upward pattern with a negative Eu anomaly (Figure 7D).
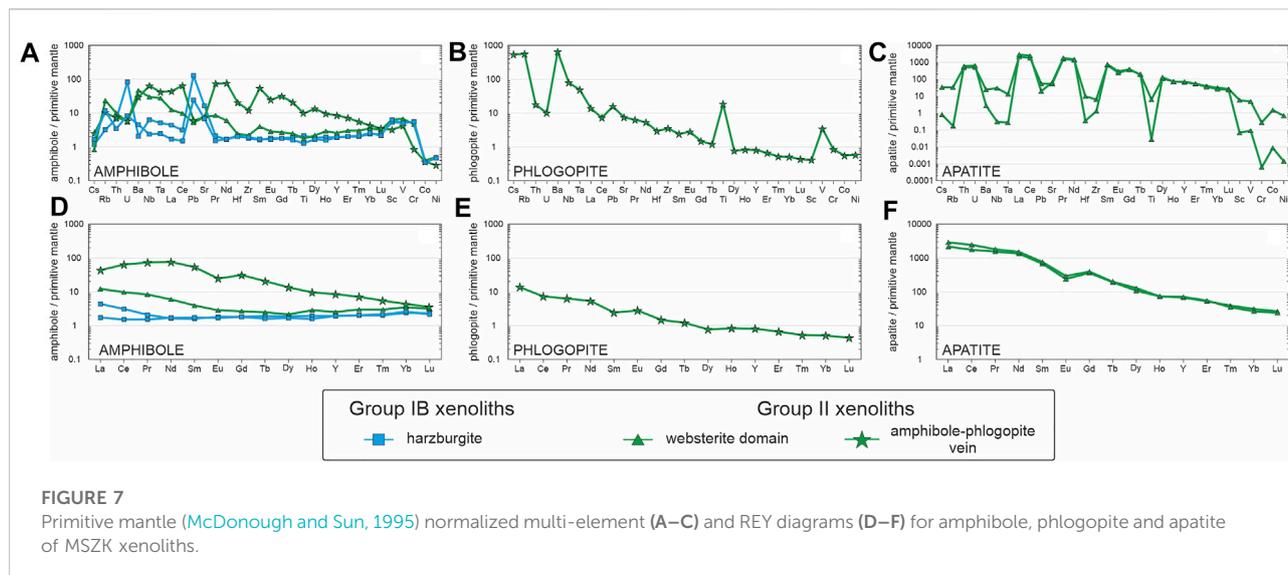
FIGURE 7
Primitive mantle (McDonough and Sun, 1995) normalized multi-element (A–C) and REY diagrams (D–F) for amphibole, phlogopite and apatite of MSZK xenoliths.

Phlogopites show enrichment in highly incompatible elements such as Cs, Rb and Ba (Supplementary Table S10; Figure 7B), but also in Ti and V. The REY diagram displays a gradual concentration decrease from LREE towards heavy rare earth elements (HREE) (Figure 7E). Apatites are extremely enriched in incompatible trace elements (Supplementary Table S10; Figure 7C). Their distribution shows depletions in HFSE elements, Pb and Sr (Figure 7C). The very high REY concentrations are characterized by very strong enrichment of LREE, which are >1,000 times higher than their PM values of McDonough and Sun (1995) (Figure 7F).

5.3 Whole-rock geochemistry

5.3.1 Major elements

Whole-rock compositions of the MSZK xenoliths (Supplementary Table S11) were determined based on mass balance calculations using the xenolith modal composition and the average mineral compositions.

The Group IA and IB single-lithology harzburgite xenoliths, and harzburgitic domains of the Group II xenoliths have homogenous whole-rock compositions (Supplementary Figure S4). In contrast, the dunite domain of xenolith MSZK1301D has higher MgO and lower SiO_2 and Al_2O_3 contents compared to the harzburgites. The Group IB olivine-orthopyroxenite, and Group II orthopyroxenite and websterite domains have lower MgO, but higher SiO_2, TiO_2, and Al_2O_3 contents with respect to the harzburgites (Supplementary Figure S4). The geochemical trend defined by the harzburgites differs from those of peridotite residue after batch and fractional melting (Supplementary Figure S4).

5.3.2 Rare earth elements + yttrium

Whole-rock REY contents of the MSZK xenoliths were estimated by mass balance calculations and shown in Supplementary Table S11. Olivine, spinel and orthopyroxene compositions were estimated from clinopyroxene concentrations and mineral/cpx partition relationships using $D^{mineral/melt}$ values of Ionov et al. (2002) and references therein. Yttrium results were calculated from Yb data based on their distribution in primitive mantle (Y concentration is ~9.75 times more than Yb concentration) (McDonough and Sun, 1995).

According to the results, the websterite domains and the amphibole-phlogopite vein from Group II xenoliths have the highest REY concentrations. These domains show convex-upward pattern with a negative Eu anomaly (Supplementary Figure S5). The orthopyroxenite and harzburgite lithologies of Group II xenoliths have lower REY concentrations. The patterns of these domains are similar to those depicted by the websterites and the amphibole-phlogopite vein with the exception of the orthopyroxenite in xenolith MSZK1306B, which shows depletion in LREE (Supplementary Figure S5). The Group I xenoliths show flat or slightly LREE-enriched characters (Supplementary Figure S5). The slightly higher LREE and HREE contents compared to elements from Sm to Tb appear in multiple xenoliths, resulting in U-shaped patterns.

6 Discussion

6.1 Formation of group IA xenoliths

6.1.1 The reactive origin of the group IA xenoliths

Group IA includes four single-lithology harzburgite xenoliths (MSZK0701; MSZK1301A; MSZK1301B;

MSZK1310) and dunite domain of the composite xenolith MSZK1301D (Table 1).

The formation of orthopyroxene-rich mantle volumes is often explained by melt extraction and accompanying mantle depletion (e.g., Dick et al., 1984; Puziewicz et al., 2015). Alternatively, orthopyroxene enrichment can be a result of a melt-rock reaction between the lherzolitic wall rock and silica-rich agents leading to reactive harzburgites (e.g., Kelemen et al., 1992, 1998; Smith et al., 1999).

The orthopyroxene modes can be a powerful tool used to explain the origin of the harzburgites. This is because the residual orthopyroxene enrichment triggered by mantle melting is relative, driven by the consumption of clinopyroxene and spinel to a lesser extent (e.g., Hirschmann et al., 1998). In contrast, newly-formed orthopyroxene grains appear in reactive harzburgites at the expense of clinopyroxene (e.g., Zheng et al., 2001) or olivine (e.g., Arai et al., 2003, 2004). In the studied MSZK harzburgites, orthopyroxene contents are high and range between 12–52 vol% (with an average of 22 vol %) (Table 1.), which rather implies reactive origin. Such orthopyroxene-rich lithologies along with subordinate clinopyroxenes (≤4.5 vol%) require high-degree partial melting (>25%), which is irreconcilable with the proposed Cenozoic evolution of the CPR (Szabó et al., 2004). The reactive origin of harzburgites is further supported by the bulk rock major element trends (e.g., positive correlation between MgO vs. Na_2O and MgO vs. FeO) of the MSZK harzburgites differing significantly from the trends of partial melting of Niu (1997) (Supplementary Figure S4). Similarly, the variably enriched trace element patterns of bulk rocks (Supplementary Figure S5) and clinopyroxenes (Figures 6D–F) are irreconcilable with mantle depletion (Niu, 2004) as depleted mantle rocks are typically strongly diluted of highly incompatible trace elements.

The presence of numerous tiny (10–50 µm), elongated or rounded spinel inclusions hosted by orthopyroxenes in the MSZK harzburgites (Figures 3F,G) also cannot be explained by depletion via partial melting, because it never leads to spinel crystallization. Additionally, these inclusions are unlikely to form during mineral breakdown reaction (e.g., garnet) or exsolution because other phases (e.g., clinopyroxene) or pseudomorphs of the decomposing phase would also be expected to appear in such scenario (Falus et al., 2000). However, the metasomatic effect of silica-enriched fluids may play a key role in forming symplectitic intergrowth of orthopyroxene and spinel as proposed by Johan et al. (2017). Also note that the high amounts of Al_2O_3 (>5 wt%) and Cr_2O_3 (>5 wt%), which is required for subsolidus exsolution of spinel inclusions, is impossible to be incorporated in orthopyroxenes. Spinel inclusions, although less frequently, were also described in olivines of harzburgites (Figure 3G), similarly as in reactive harzburgites from Kamchatka (Arai et al., 2003) and the Philippines (Arai et al., 2004).

All prior considerations suggest that the MSZK harzburgites have a reactive origin. This orthopyroxene enrichment fits the definition of stealth metasomatism (O'Reilly and Griffin, 2013). Since there are no microstructures showing reaction (e.g., secondary orthopyroxene appearing at the expense of olivine or clinopyroxene) in the MSZK xenoliths, it is challenging to determine the precursor rock composition. Nevertheless, the MSZK harzburgites are among the BBHVF xenoliths with the highest olivine contents (dominantly >70 vol%; Figure 2). Thus, the dissolution of clinopyroxene may occur at larger amounts than that of olivine. This potentially implies a lherzolitic precursor, a lithology rare in MSZK xenoliths (Créon et al., 2017b), but frequent in other BBHVF localities (Figure 2). The possible reason why the metasomatism leaves no precursor lherzolites in MSZK locality is its pervasive style.

The only non-harzburgite lithology belonging to the Group IA is the dunite domain of the composite xenolith MSZK1301D (Table 1). It is adjacent to an olivine-orthopyroxenite domain with a well-defined contact zone between them (Figure 3A). Dunite veins in harzburgite are widely interpreted as intensive reactions between olivine-saturated melts and orthopyroxene-rich wall rocks (e.g., Kelemen et al., 1995). This suggests that the formation of the dunite vein may have followed the formation of the olivine-orthopyroxenite domain. Since intensive melting of the pyroxenes during metasomatic reactions requires high melt-rock ratios, dunite veins could represent possible melt migration pathways (Yoshikawa et al., 2018) as it was verified by experiments as well (Morgan and Liang, 2005). This interpretation can be applied to the dunite domain of the xenolith MSZK1301D because of the coarse granular texture dominated by stress-free olivines (Figure 3A). Note, however, that recrystallization after the magmatic event can result in similar petrographic features and also explains the lack of reaction textures in other Group I xenoliths.

6.1.2 Possible melt agent forming the group IA xenoliths

Orthopyroxene-enrichment via metasomatism requires silica-rich, orthopyroxene-saturated melts. Such melts appear most commonly in volcanic arc environments. Beneath volcanic arcs, the liberation of fluids from a subducting slab can trigger partial melting in the mantle wedge overlying the slab (e.g., Iwamori, 1998; Grove et al., 2006). These melts formed at high pressure saturate first in olivine only, leading to the dissolution of pyroxenes during melt-rock reactions and the formation of dunites (Kelemen et al., 1992). However, ongoing melt-rock reactions can lead to gradual modification of the melt from basalt to basaltic andesite composition, resulting in orthopyroxene saturation (Morgan and Liang, 2005) at lower pressure in constant temperature circumstances (Kelemen et al., 1992). This process can explain the co-precipitation of orthopyroxene and olivine with simultaneous clinopyroxene dissolution; in other words, the formation of harzburgites

FIGURE 8
Relationship between **(A)** Al-Cr-Fe^{3+} in spinel (supra-subduction spinels are based on Arai et al., 2004); **(B)** Al_2O_3 vs. CaO in orthopyroxene (supra-subduction orthopyroxenes are based on Arai and Ishimaru, 2008); **(C)** Ti/Nb vs. Zr/Nb in amphibole (supra-subduction and intraplate amphiboles are based on Coltorti et al., 2007) for studied MSZK xenoliths.
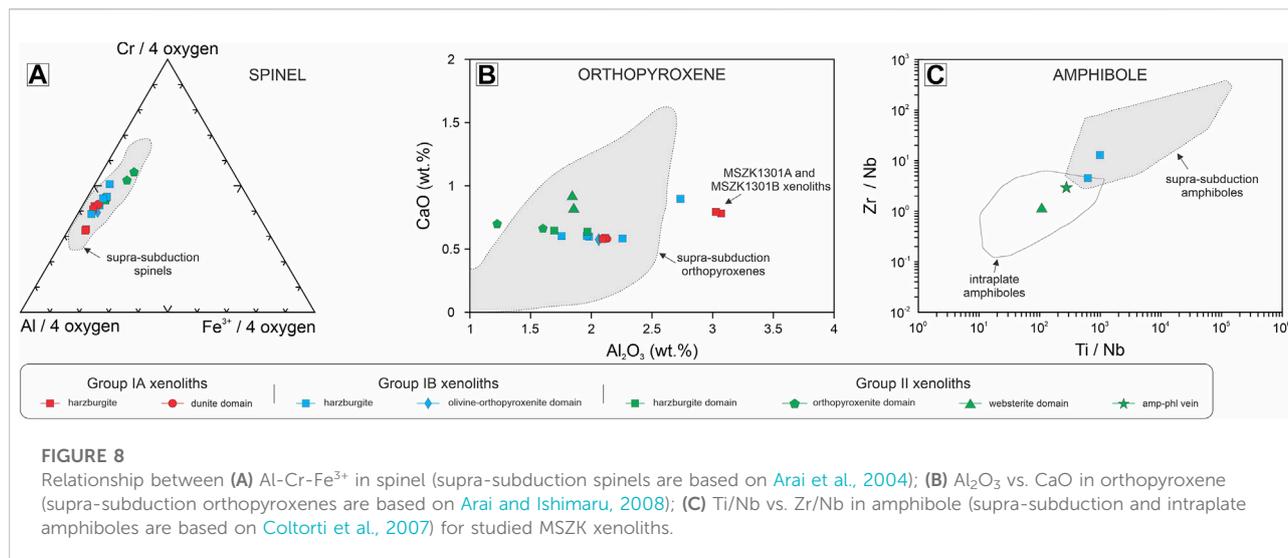
(Kelemen et al., 1998), even when the magma mass is decreasing (Kelemen et al., 1992).

The migration of silica-rich (even quartz-oversaturated) melts is not unprecedented in the BBHVF. Bali et al. (2008) described a highly unusual quartz-bearing orthopyroxene-rich websterite xenolith from Szigliget (~10 km southwest of Mindszentkálla; Figure 1B). The quartz appeared as rounded or needle-shaped crystal inclusions in orthopyroxenes and was interpreted to have co-crystallized with its host. The quartz-bearing xenolith was also rich in silicate melt inclusions (SMIs) hosted by pyroxenes. The metasomatic melt represented by the primary SMIs was found to be rich in SiO_2 (66–72 wt%) -and alkalis, and poor in MgO, FeO and CaO. Furthermore, it was strongly enriched in LREE and large ion lithophile elements (LILE), and displayed negative Nb, Ta and Sr and slightly positive Pb anomalies. These geochemical characteristics led Bali et al. (2008) to conclude that a quartz-saturated silicate melt was released from metasedimentary rocks of a subducted oceanic slab. Other studies also suggested migrating subduction-related melts beneath the BBHVF (e.g., Downes et al., 1992; Bali et al., 2002, 2007), occasionally evidenced by silica-rich (>55 wt%) glass veins (Créon et al., 2017b).

We suggest that beneath MSZK, subduction-related extensive metasomatism was caused by a silica-rich, orthopyroxene-saturated melt. In addition to the metasomatism-induced orthopyroxene enrichment, several lines of geochemical evidence point to the supra-subduction zone (SSZ) origin of the MSZK harzburgites. The most important geochemical characteristics are the high Mg# (>0.90; Figures 4B,C) and low Al_2O_3 in orthopyroxenes (mostly <2.5 wt%; Supplementary Figure S3C), as well as the Cr_2O_3-rich spinels (>29 wt%; Figure 8A). The presence of clinopyroxenes displaying U-shaped REY patterns (Figures 6D,E) is also in accordance with SSZ environment (Parkinson

and Pearce, 1998). However, the LREE and HREE enrichment compared to Eu, Gd, Tb depletion is not as pronounced (Figures 6D,E) as in other BBHVF xenoliths (Bali et al., 2007; Dobosi et al., 2010; Berkesi et al., 2012; Embey-Isztin et al., 2014). The only Group I xenoliths showing no U-shaped REY patterns are MSZK1301A, MSZK1301B and MSZK1311 samples. The latter two xenoliths are also located outside the field constrained by SSZ xenoliths on the Al_2O_3-CaO diagram of orthopyroxenes (Figure 8B). The reason for this geochemical deviation from the rest of the Group I xenoliths could be due to the influence of a basaltic melt (probably the same as the one responsible for the formation of Group II xenoliths; see chapter 6.3), based on enrichment of these two xenoliths in some basaltic elements (Ti, Al, Fe in clinopyroxene; Ti, Al and Ca in orthopyroxene; Al in spinel). Note that one single-lithology harzburgite xenolith (MSZK1309) in Group I shows a positive Eu anomaly (Figure 6E). Such a positive anomaly is commonly explained by the dissolution of plagioclase in the subducting oceanic crust (Dai and Zheng, 2019), which is in agreement with the proposed evolution of that xenolith.

6.2 Formation of group IB xenoliths

Group IB, similarly to Group IA, includes orthopyroxene-rich lithologies, namely six single-lithology harzburgites (MSZK0702; MSZK1301C; MSZK1302; MSZK1307; MSZK1309; MSZK1311) and the olivine-orthopyroxenite domain of the composite xenolith MSZK1301D (Table 1). The Group IB xenoliths are characterized by high U, Pb and Sr concentrations in clinopyroxenes, showing positive anomalies on the normalized multi-element diagram (Figure 6B). In contrast, Group IA xenoliths lack these anomalies (Figure 6A). Among these elements, Pb enrichment is

FIGURE 9
Relationships between **(A)** Pb/Ti vs. U/Ti; **(B)** Pb/Ti vs. Nb/U; **(C)** U/Zr vs. Ti/Nd; **(D)** Pb/Hf vs. Pb/Ta; **(E)** Sc/Lu vs. Ti **(F)** Pb/Ti vs. $T_{Ca-in-opx}$, where all trace element composition and ratios refer to clinopyroxenes. Thermometer of $T_{Ca-in-opx}$ is after Nimis and Grütter (2010). Published Bakony-Balaton Highland Volcanic Field (BBHVF) upper mantle xenoliths: Embey-Isztin et al., 1989; 2001; 2014; Downes et al., 1992; Bali et al., 2002; 2007; 2008; Hidas et al., 2007; 2010; Nédli et al., 2009; Dobosi et al., 2010; Berkesi et al., 2012; Créon et al., 2017b. Worldwide supra-subduction xenoliths with Pb positive anomalies are taken from Grégoire et al., 2001; Ishimaru et al., 2007; Aradi et al., 2020.

particularly unusual in the upper mantle. However, in subduction zones, where crustal rocks are recycled to the mantle, Pb is transported to sub-Moho depths in large amounts. The main factor of Pb distribution in the lithosphere is its highly incompatible behavior during mantle melting (e.g., Hauri et al., 1994), thus Pb is delivered to the crust by melts, resulting in its enrichment above the Moho and depletion beneath it. Another phenomenon leading to increased Pb concentrations in the crust is the radioactive decay of U. Since U is a highly incompatible element as well (e.g., Hauri et al., 1994), magmatism gradually increases its concentration from the mantle towards the crust. Further U enrichment in the oceanic crust can be attributed to its hydrothermal alteration (Staudigel, 2003). According to Tenthorey and Hermann (2004), sediments are the major host of Pb in the oceanic crust, however altered oceanic crust basalts also contain significant amounts of Pb. Regelous et al. (2010) showed that subducting sediments and altered oceanic crust basalts release Pb-bearing aqueous fluids or hydrous melts at shallower and greater depths, respectively, within the subduction zone. These agents transport notable amounts of Pb from different sources to the mantle wedge (Chauvel et al., 1995; Saha et al., 2005) leading to Pb-enriched lavas (Miller et al., 1994) and peridotite xenoliths originating from such environment (Grégoire et al., 2001; Ishimaru et al., 2007; Aradi et al., 2020).

The difference between Group IA and IB xenoliths is best highlighted by U-Pb vs. Ti-HFS element ratios (e.g., U/Ti; U/Zr; Nb/U; Pb/Ti; Pb/Ta; Pb/Hf) (Figure 9). The Group IB xenoliths have higher U/Ti, U/Zr, Pb/Ti, Pb/Ta; Pb/Hf and lower Nb/U ratios compared to Group IA xenoliths (Figure 9). The ratios peculiar to Group IB xenoliths match with xenoliths from areas with ongoing (Papua New Guinea: Grégoire et al., 2001; Kamchatka: Ishimaru et al., 2007) or ceased subductions (Styrian Basin: Aradi et al., 2020) (Figure 9.). If the oceanic crust and the related subducted materials are rich in Pb and U, the subducted materials are not enriched in HFSE (Bebout, 2007). Therefore, the subducted oceanic materials normally have high U-Pb vs. Ti-HFS ratios. These ratios do not change dramatically during fluid liberation, since U and Pb partition into the fluids, whereas HFSE and Ti preferentially remain in the solid at a lower temperature (<1,000°C) up to high pressures (4 GPa) (Keppler, 1996; Manning, 2004; Kessel et al., 2005; Hermann et al., 2006). Therefore, migrating fluids can extend these characteristic element ratios to the mantle wedge. Strontium, whose solubility is high in aqueous fluids in high p-T conditions (900–1,200°C, 4–6 GPa; Kessel et al., 2005), is also enriched in Group IB xenoliths compared to Group IA (Figure 6). The REE, especially from Sm to Lu, is similar to HFS and Ti, and prefer to remain in the solid phase and barely soluble in aqueous fluids (Kessel et al., 2005). Nevertheless, Ti/LREE (especially Ti/Nd) ratio is a reliable

tool to discriminate between Groups IA and IB (Figure 9C), and so is the ratio of Sc/Lu (Figure 9E).

All these imply that the upper mantle represented by Group IB xenoliths experienced metasomatism by subduction-related aqueous fluids. More than half of the Group I xenoliths shows U, Pb and Sr enrichment (i.e., belong to the Group IB subgroup) (Table 1). This suggests that the fluid infiltration likely followed the orthopyroxene enrichment (melt metasomatism), but was restricted to a smaller mantle volume. Since both the melt and fluid metasomatism are assumed to have happened in a mantle wedge environment, they are likely linked to the same subduction event. The Group IB xenoliths generally have equilibration temperatures ($T_{Ca-in-opx}$: 899–1,016 with an average of 919°C) similar to the Group IA xenoliths ($T_{Ca-in-opx}$: 897–986 with an average of 934°C) (Figure 9F; Table 1), implying that both melt and fluid metasomatism affected the mantle wedge in similar depth ranges. The akin equilibration temperatures may also suggest that the fluid infiltration did not affect the Ca content of the rocks.

Two Group IB harzburgite xenoliths (MSZK0702; MSZK1307) contain minor pargasitic amphibole (≤1 vol%; Table 1) within melt pockets (Supplementary Figure S2A). Based on the high Ti/Nb (>600) and Zr/Nb (>4) ratios of these amphiboles, their formation is suggested to link to SSZ environments (Figure 8C; Coltorti et al., 2007). These amphiboles are enriched in U, Pb and Sr (Figure 7A) similarly to the Group IB clinopyroxenes. Along with the lack of REY enrichment (Figure 7D), these geochemical signatures suggest that the amphibole formation is likely related to the fluid metasomatism.

The only non-harzburgite lithology belonging to the Group IB is the olivine-orthopyroxenite domain of the composite xenolith MSZK1301D (Table 1). The reason of the higher orthopyroxene content of this domain could be explained by the modal composition of the precursor. If it is assumed that clinopyroxene is the major mineral that was converted to orthopyroxene during the metasomatism, as it was proposed in section 6.1.1., then the olivine-clinopyroxenite described from the Szentbékkálla locality of BBHVF earlier (Figure 1B; Bali et al., 2002; Falus et al., 2004) is an appropriate candidate for such a precursor.

The reason why the olivine-orthopyroxenite domain shows fluid metasomatism-related U, Pb and Sr enrichment (i.e., belonging to Group 1B; Figure 6B), while its neighboring dunite lacks it (Figure 6A) is probably due to textural characteristics. Clinopyroxene in the dunite domain only appears as small inclusions (40–60 μm) hosted by large olivine grains (>500 μm) (Supplementary Figure S2B). The olivine hosts might have hindered direct contact between the fluid agent and the clinopyroxenes by acting as a physical barrier. This interpretation is further supported by the generally slow diffusion rate for trace elements in the olivine structure (Spandler and O'Neill, 2010).

6.3 The formation of group II xenoliths

6.3.1 General observations and their implications in group II xenoliths

Group II xenoliths consist of variable lithologies (harzburgite, orthopyroxenite, websterite) of two composite xenoliths (MSZK1305; MSZK1306B) (Table 1). Generally, these lithologies have higher Ti, Mn, Ca and lower Si, Cr, Ni, and Mg# compared to those of Group I (Figure 4; Supplementary Figure S3). The enrichment in basaltic elements is weak in the harzburgite, moderate in the orthopyroxenite and significant in the websterite domains (Figure 4; Supplementary Figure S3). These characteristics, along with the convex-upward REY patterns of clinopyroxenes (Figure 6F), point to an interaction with mafic melts. However, the lack of melt infiltrations, reaction coronas and compositional zoning at the margins of the MSZK xenoliths all suggest that the host basalt is likely not the metasomatic agent. This is further supported by the fact that xenoliths were collected from pyroclastic sequences (Supplementary Figure S1B), which can preserve the original physical and chemical properties of the xenoliths better, due to their fast cooling on the surface.

A general geochemical feature in all lithologies of Group II xenoliths is the negative Eu anomaly (Figure 6F). It may either be related to the crystallization of plagioclase during magma evolution, or to redox state changes affecting the distribution of Eu compared to other REE (Griffin and O'Reilly, 2007). The alkali basaltic melts in the BBHVF originate from the asthenosphere far deeper than the stability field of plagioclase (e.g., Embey-Isztin et al., 1993), thus residual plagioclase retaining Eu in the source region is out of option. In the BBHVF, only one upper mantle xenolith is reported containing plagioclase (Embey-Isztin, 1976), hence the mass accumulation of plagioclase in the lithospheric mantle is also unlikely. Therefore, it is suggested that the negative Eu anomaly results from changing redox conditions of the melt during its upward migration.

6.3.2 Origin of harzburgite domains within group II composite xenoliths

The harzburgite domains in Group II composite xenoliths likely represent a mantle volume originally belonging to Group I, subsequently affected by a younger event. This is based on the observation that petrographic features, including modal composition and textural characteristics, do not differ in the single-lithology harzburgites and the harzburgite domains of composite xenoliths (Figure 3; Supplementary Figure S4; Table 1), implying a common origin for them. However, they have several different geochemical features as follows. The harzburgite domains of the composite xenoliths are out of the OSMA (olivine-spinel mantle array; Arai, 1994) range (<87 forsterite content in olivine along with 0.47–0.48 Cr# in spinel; Figure 4A). Furthermore, they are among the harzburgites

with the lowest Mg# in their pyroxenes (~0.88 and ~0.91 Mg# for orthopyroxene and clinopyroxene, respectively; Figures 4B–E). The subordinate clinopyroxenes in harzburgite xenoliths have lower REY contents (6–24 ppm ΣREY; Figures 6D,E; Supplementary Table S9) compared to the harzburgite domains of composite xenoliths (~148 ppm ΣREY; Figure 6F; Supplementary Table S9). The other difference is the REY pattern showing flat and enriched distributions in the former (Figures 6D,E) and convex-upward distribution in the latter group (Figure 6F). All these geochemical features suggest that the single-lithology harzburgites and the harzburgite domains of composite xenoliths have different evolution.

The convex-upward pattern of clinopyroxenes in harzburgite domains of the composite xenoliths is also characteristic for clinopyroxenes of the orthopyroxenite and websterite domains in composite xenoliths (Figure 6F). This similarity suggests that the younger geochemical event, presumably linked to mafic melts, that likely added the orthopyroxenite and websterite lithologies to the mantle volume, overprinted the trace element characteristics of the neighboring parts of the presumably older harzburgites via chromatographic processes (Navon and Stolper, 1987), leading to cryptic metasomatism (Dawson, 1984). In other words, the harzburgite host rock of the composite xenoliths likely failed to preserve its original trace element attributes during the formation of orthopyroxenite and websterite lithologies.

6.3.3 The formation of orthopyroxenites within group II composite xenoliths

The orthopyroxenite lithology, albeit in a subordinate amount, is present in various settings below the Moho, including ophiolitic mantle (e.g., Le Roux et al., 2014) orogenic peridotites (e.g., Malaspina et al., 2006) and upper mantle xenoliths (e.g., Chen and Zhou, 2005; Wang et al., 2008). Most of the studies explain the formation of orthopyroxenites with melt/fluid and peridotite interactions based on resorbed olivines. Several studies suggest that siliceous melts and fluids derived from an oceanic slab could be the most probable metasomatic agents responsible for orthopyroxenite formation (Ertan and Leeman, 1996; Chen and Zhou, 2005). Indeed, orthopyroxene-rich reactive boundary layers were described to form between basaltic andesite melt and peridotite at high pressure (≥2.5 GPa) and temperature (≥1,375 °C) (Mallik and Dasgupta, 2012). However, the crystallization of orthopyroxene-oversaturated reacting melt prevents further melt-rock reactions (Wang et al., 2016). Alternatively, reactions between hydrous ferro-basalt and peridotite in upper mantle conditions (0.8–2 GPa; 1,250–1,385°C) can also lead to the formation of orthopyroxenites as suggested by experimental runs of Wang et al. (2016). Based on their model, the diffusion of water from the hydrous melt into the host peridotite can induce melting in the peridotite, resulting in olivine-rich residues. The mixing of the

migrating melt with the melt produced in the host rock results in a third, hybrid melt. This hybrid melt is responsible for the olivine dissolution and orthopyroxene precipitation along the melt-rock interface. Other studies on natural samples also emphasize the possible role of basaltic melt (Arai et al., 2006) and water (Smith et al., 1999; Tamura and Arai, 2006) in the formation of orthopyroxenites. The significance of water is further supported by the common appearance of hydrous phases such as amphibole or phlogopite in orthopyroxenites (Ertan and Leeman, 1996; Chen and Zhou, 2005). The reacted melts assumed to contribute to orthopyroxenite formation have similar water contents in experimental runs (0.61–0.66 wt%; Wang et al., 2016) and natural samples (0.57–1.24 wt%; Arai et al., 2006). Note that orthopyroxenite lithology was only described from the Little Hungarian Plain Volcanic Field (LHPVF; Figure 1A) in the CPR so far (Szabó et al., 1995).

In the MSZK composite xenoliths, the growth of orthopyroxene of the orthopyroxenite domain at the expense of olivine of the neighboring harzburgite domain (Figures 3B,C) suggest that the orthopyroxenite domain was formed later than the harzburgite host rock. It also means that the websterite domains and the amphibole-phlogopite vein, which are in contact with the orthopyroxenite domains only (Figures 3B,C), must have formed after the harzburgite parts.

As it was indicated before, we also suggest that mafic melts are responsible for the orthopyroxenite formation beneath the MSZK locality, based on their basaltic element enrichment (Figure 4; Supplementary Figure S3) and convex-upward REY patterns of clinopyroxenes (Figure 6F). Analyses concluded high water contents for the BBHVF basalts (2.0–2.5 wt%; Kovács et al., 2020), which is capable promoting orthopyroxenite vein formation in the mantle according to the experiments of Wang et al. (2016). Furthermore, the upward-moving basaltic melts likely contacted harzburgite volumes beneath the MSZK locality, which were produced by orthopyroxene enrichment during a previous metasomatism by subduction-related melts and fluids. The dissolution of the orthopyroxenes resulted in more evolved melt compositions, and possible orthopyroxene-saturation and even oversaturation after interacting with large volumes of harzburgite. These processes resulted in the orthopyroxenite formation. The role of harzburgite lithology, as a source of melts responsible for the formation of orthopyroxenite veins, was also highlighted by Bénard et al. (2022). Without orthopyroxene dissolution, basaltic melts would remain orthopyroxene undersaturated with their movement restricted to the olivine-clinopyroxene cotectic line on schematic olivine-clinopyroxene-SiO_2 phase diagram (Kelemen, 1990).

We estimated the equilibrium melt composition for orthopyroxenites as well, using clinopyroxene-basaltic melt and orthopyroxene-basaltic melt distribution coefficients (Ionov et al., 2002; Adam and Green, 2006) (Figure 10A). The estimated equilibrium melt compositions (Supplementary Table

S12) show the best fit with SMI reported by Szabó et al. (2009) (Figure 10A). These SMI are hosted by amphibole-bearing spinel lherzolite xenoliths from Szigliget (Figure 1B). The trapped SMI likely represent a melt with a trace element content similar to that of the host alkali basalts, but more enriched in silica (Szabó et al., 2009). According to Szabó et al. (2009), such melt may have formed by the interaction between an alkali mafic melt rising from the asthenosphere and a mantle portion previously metasomatized by a slab-derived melt. This evolution history is very similar to what we suggest for the melt responsible for the orthopyroxenite formation in the upper mantle beneath the MSZK locality. Note that the trace element composition of several studied SMI shows enrichment in U and Pb (Szabó et al., 2009), a feature also characteristic of the Group IB harzburgites of the MSZK xenoliths (Figure 6B). These properties were likely inherited from the metasomatized mantle wedge harzburgites representing the wall rocks next to the upward migrating mafic melts.

6.3.4 The formation of websterites and amphibole-phlogopite vein within group II composite xenoliths

The appearance of websterite followed the orthopyroxenite formation, as indicated by resorbed orthopyroxenes in the latter along the contact zone (Figure 3D). The large (3,000–5,000 μm), tabular, stress-free clinopyroxenes of the websterites, with enclosed orthopyroxenes, amphiboles and apatites (Figure 3D), are petrographic features typical of cumulates representing crystallized products (e.g., Perinelli et al., 2017). The enrichment of basaltic elements in the rock-forming minerals of the websterites is even higher compared to the orthopyroxenites (Figure 4; Supplementary Figure S3). Together with the convex-upward REY patterns of clinopyroxenes (Figure 6F), this suggests that websterite formation is related to mafic melts. To further test this hypothesis, the equilibrium melt of websterites was estimated with the use of distribution coefficients for clinopyroxene-basaltic melt and orthopyroxene-basaltic melt (Ionov et al., 2002; Adam and Green, 2006) (Figure 10B). The resulting equilibrium melt composition shows the best overlap with basaltic melts defined by the SMIs in the study of Szabó et al. (2009) (Figure 10B), similarly to what was found for the MSZK orthopyroxenites described above (Figure 10A).

Clinopyroxene is often the liquidus phase in basalts beneath the crust, leading to the formation of clinopyroxene-rich lithologies upon crystallization (e.g., Downes et al., 2004). Thus, the dominance of clinopyroxene in the websterites (~70 vol%) suggests that they could represent crystallized melt migration paths. The significant modal abundance of orthopyroxenes (~30 vol%) in the MSZK websterites can be explained by the incomplete alteration of orthopyroxenites or by orthopyroxene dissolution and subsequent orthopyroxene saturation in the basaltic melt. The higher equilibration

FIGURE 10
Estimated trace element composition of melt responsible for the formation of **(A)** orthopyroxenite and **(B)** websterite domains of composite xenoliths (MSZK1305; MSZK1306B). The silicate melt-orthopyroxene/clinopyroxene partition coefficients are taken from Ionov et al. (2002) and Adam and Green (2006). Primitive mantle (PM) (McDonough and Sun, 1995) normalized trace element distributions are compared to trace element compositions of melt modelled from Bakony-Balaton Highland Volcanic Field (BBHVF) xenoliths (Bali et al., 2008; Szabó et al., 2009). Abbreviations: opx–orthopyroxene; cpx–clinopyroxene; smi–silicate melt inclusion; mp–melt pocket.

temperatures of websterites (T_{NG}>1,000°C; T_{REE}>1,100°C) compared to orthopyroxenites (T_{NG}<1,000°C; T_{REE}<1,100°C) (Table 1) further indicate that melt crystallization is a more important process in websterite formation than melt-rock reactions, which often result in lower temperatures due to the mixing of melt with the colder wall rocks. All these suggest that the MSZK websterites likely represent mafic melts crystallized along melt channels. This is consistent with other studies interpreting websterite veins as products appearing along recrystallization fronts of pervasive melt migration channels (Garrido and Bodinier, 1999; Dantas et al., 2009).

The amphibole-phlogopite vein crosscutting the orthopyroxenite domain of xenolith MSZK1305 (Figure 3C) is likely a product of the last event in the upper mantle of the study area. It is possibly derived from the mafic melt that went through high-degree fractional crystallization and became highly enriched in incompatible elements (Figure 7). Amphibole-rich veins with similar proposed origin were found in composite xenoliths from Szigliget (Embey-Isztin, 1976; Bali et al., 2018) (Figure 1B).

6.4 Possible links between metasomatic events and the evolution of the Carpathian-Pannonian region

Based on the above-described observations, two events can be distinguished in the upper mantle beneath the MSZK locality (Figure 11). The first event is related to the migration of subduction-related melts and fluids leading to the formation of harzburgitic lithologies (Figure 11) and enrichment in fluid mobile elements such as U, Pb and Sr. The orthopyroxene grains in the

MSZK harzburgites are subhedral with generally large grain size (500–1,000 μm). This is in contrast with newly-formed orthopyroxenes in reactive harzburgites, which often show fibrous texture, especially in areas with active volcanism related to ongoing subduction (McInnes et al., 2001; Arai et al., 2004). The well-equilibrated equigranular (Figure 3G) and coarse granular (Figure 3H) textures of the MSZK harzburgites suggests that the orthopyroxene enrichment is an event predating potential mantle equilibration (i.e., recrystallization and annealing). Such process could have been facilitated by the increased heat from the asthenospheric updoming during the extension in the central CPR (Horváth, 1993). Thus, the orthopyroxene enrichment is thought to have happened before the Neogene. This is further supported by Paleogene igneous rocks in the vicinity of the Middle Hungarian zone (MHZ) which have subduction-related characteristics (e.g., Pb enrichment) (Benedek et al., 2004). The influence of subduction-related melts and fluids leading to orthopyroxene enrichment in the subcontinental mantle occurs in some xenoliths in Szigliget (Bali et al., 2008) and Tihany localities (Berkesi et al., 2012) in the westernmost and in the easternmost part of the BBHVF, respectively (Figure 1B) as well as in sampling sites between them (Bali et al., 2007) such as the MSZK locality. This distance of at least 35 km suggests that the subduction was a regional event with major modification to the affected mantle volume. Note that a restricted number of harzburgites with possible reactive origin were also described from the LHPVF (Szabó et al., 1995), which is situated in the vicinity of BBHVF (Figure 1A).

During the Cenozoic, significant lateral tectonic movements (extrusion, rotations) occurred in the CPR (e.g., Csontos, 1995). It is assumed that during this tectonic evolution the lithospheric mantle
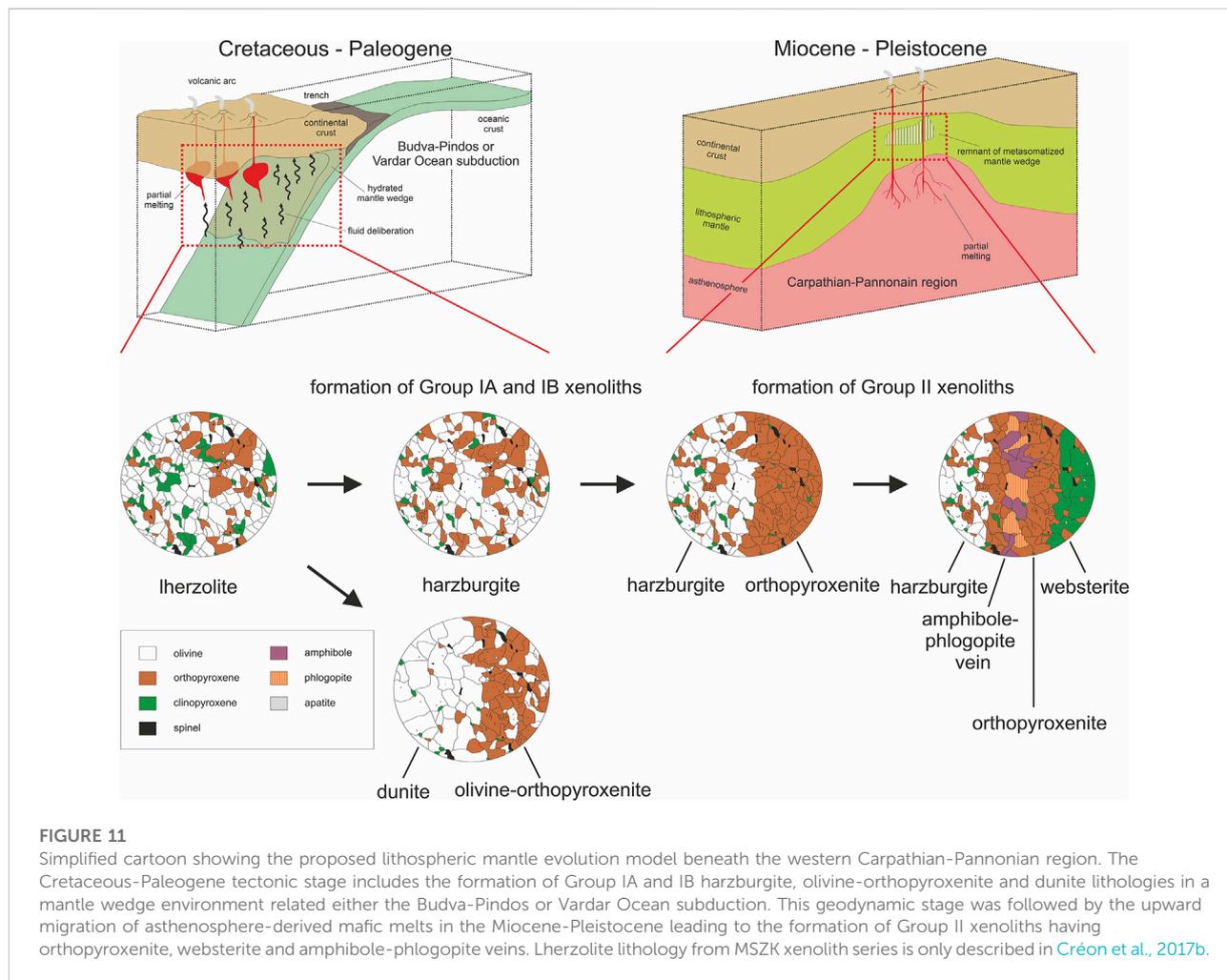
FIGURE 11
Simplified cartoon showing the proposed lithospheric mantle evolution model beneath the western Carpathian-Pannonian region. The Cretaceous-Paleogene tectonic stage includes the formation of Group IA and IB harzburgite, olivine-orthopyroxenite and dunite lithologies in a mantle wedge environment related either the Budva-Pindos or Vardar Ocean subduction. This geodynamic stage was followed by the upward migration of asthenosphere-derived mafic melts in the Miocene-Pleistocene leading to the formation of Group II xenoliths having orthopyroxenite, websterite and amphibole-phlogopite veins. Lherzolite lithology from MSZK xenolith series is only described in Créon et al., 2017b.

was coupled to the crust (Kovács and Szabó, 2008). This means that the pre-Neogene mantle events and volcanic episodes happened at different geographic locations than their current position. Kovács et al. (2007) and Kovács and Szabó (2008) argued that igneous rocks and xenoliths in the vicinity of the Middle Hungarian zone (MHZ) (Figure 1A) are related to the subduction of either the Budva-Pindos or Vardar Ocean during the Mesozoic-Paleogene (Csontos and Vörös, 2004). This model suggests that the subduction-modified lithospheric mantle was coupled to the crust during the extrusion of the ALCAPA microplate.

The second metasomatic event can be linked to the migration of basaltic melt(s) in the upper mantle leading to orthopyroxenitic, websteritic and amphibole-phlogopite vein lithologies (Figure 11). It is younger than the orthopyroxene enrichment, as proved by the textural relationships of the different lithologies. It is reasonable to assume that this magmatic event manifesting in the lithospheric mantle is the same that produced the Neogene alkali basalt volcanism carrying the xenoliths to the surface (Figure 11). Most studies explain the alkali basalt volcanism with decompressional mantle melting caused by the asthenosphere upwelling subsequent

to the extension in the CPR (e.g., Embey-Isztin et al., 1993; Seghedi et al., 2004). Alternatively, a recent interpretation suggests that compression appearing in the tectonic inversion stage (~8–0 Ma) of the evolution of the CPR may have squeezed partial melts from the hydrated asthenospheric dome (Kovács et al., 2020). In both cases, the melting in the asthenosphere was followed by the upward migration of basaltic melt batches, causing interactions with harzburgitic mantle domains and vein formation in the upper mantle, shortly preceding xenolith entrapment in the host basalt.

7 Conclusion

1) Ten single-lithology harzburgite and three composite upper mantle xenoliths were studied from Mindszentkálla, central Pannonian Basin. The composite xenoliths consist of various combinations of dunite, olivine-orthopyroxenite, harzburgite, orthopyroxenite, websterite and amphibole-phlogopite domains. The evolution of these variable lithologies was linked to two major magmatic events.

2) The single-lithology harzburgites and one composite xenolith with dunitic and olivine-orthopyroxenitic domains (Group I xenoliths) were formed during the interaction between silica-rich melt and peridotitic wall rock. This event is assumed to have taken place in a mantle wedge environment.

3) Shortly after the orthopyroxene enrichment leading to the formation of harzburgite lithology with dunite veins, additional fluid infiltration occurred in some parts of the previously metasomatized mantle volumes. This led to the formation of Group IB xenoliths characterized by U, Pb and Sr enrichment in the rock-forming silicates. The fluid agent was likely liberated from the downgoing slab of the same subduction that is linked to the harzburgite formation. Contrarily, Group IA xenoliths represent mantle segments not affected by the fluid infiltration.

4) Formation of orthopyroxenite and websterite domains and amphibole-phlogopite veins of the composite xenoliths (Group II xenoliths) are related to variably evolved mafic silicate melts. The orthopyroxenites must have been formed via melt-rock reactions, whereas the websterite and amphibole-phlogopite veins are crystallized products of mafic melts.

5) Group I xenoliths are possibly linked to the subduction of either the Budva-Pindos or the Vardar Ocean during the Mesozoic–Paleogene, far from the current position of the Mindszentkálla locality, where the metasomatized lithosphere was transferred by extrusion. The Group II xenoliths represent a younger, Neogene basaltic magmatic event, possibly the same that produced the basalts transporting the xenoliths to the surface.

Data availability statement

The original contributions presented in the study are included in the article/Supplementary Material, further inquiries can be directed to the corresponding author.

Author contributions

LP, ZK, CS and IJK took part in the conceptualization of the study. ZK, NL, LEA and CS participated in the field work. LP, KH and CJG created the strategy of the geochemical analyses and processed them. LP interpreted the data and wrote the first draft of the manuscript. LP and NL compiled the figures and tables. MB contributed to the regional geological interpretation. JC helped finalizing the ideas. All authors contributed to manuscript revision, have read and approved the submitted version.

Funding

Acknowledgments

Conflict of interest

The authors declare that the research was conducted in the absence of any commercial or financial relationships that could be construed as a potential conflict of interest.

Publisher's note

All claims expressed in this article are solely those of the authors and do not necessarily represent those of their affiliated organizations, or those of the publisher, the editors and the reviewers. Any product that may be evaluated in this article, or claim that may be made by its manufacturer, is not guaranteed or endorsed by the publisher.

Supplementary material

The Supplementary Material for this article can be found online at: https://www.frontiersin.org/articles/10.3389/feart.2022.998391/full#supplementary-material

References

Adam, J., and Green, T. (2006). Trace element partitioning between mica-and amphibole-bearing garnet lherzolite and hydrous basanitic melt: 1. Experimental results and the investigation of controls on partitioning behaviour. *Contrib. Mineral. Petrol.* 152 (1), 1–17. doi:10.1007/s00410-006-0085-4

Aradi, L. E., Bali, E., Patkó, L., Hidas, K., Kovács, I. J., Zanetti, A., et al. (2020). Geochemical evolution of the lithospheric mantle beneath the Styrian Basin (western Pannonian Basin). *Lithos* 378, 105831. doi:10.1016/j.lithos.2020.105831

Arai, S., and Ishimaru, S. (2008). Insights into petrological characteristics of the lithosphere of mantle wedge beneath arcs through peridotite xenoliths: a review. *J. Petrol.* 49 (4), 665–695. doi:10.1093/petrology/egm069

Arai, S., Ishimaru, S., and Okrugin, V. M. (2003). Metasomatized harzburgite xenoliths from avacha volcano as fragments of mantle wedge of the Kamchatka arc: implication for the metasomatic agent. *Isl. Arc* 12 (2), 233–246. doi:10.1046/j.1440-1738.2003.00392.x

Arai, S., Takada, S., Michibayashi, K., and Kida, M. (2004). Petrology of peridotite xenoliths from Iraya volcano, Philippines, and its implication for dynamic mantle-wedge processes. *J. Petrol.* 45 (2), 369–389. doi:10.1093/petrology/egg100

Arai, S., Shimizu, Y., Morishita, T., and Ishida, Y. (2006). A new type of orthopyroxenite xenolith from takashima, southwest Japan: silica enrichment of the mantle by evolved alkali basalt. *Contrib. Mineral. Petrol.* 152 (3), 387–398. doi:10.1007/s00410-006-0117-0

Arai, S. (1994). Characterization of spinel peridotites by olivine-spinel compositional relationships: review and interpretation. *Chem. Geol.* 113 (3-4), 191–204. doi:10.1016/0009-2541(94)90066-3

Bali, E., Szabó, C., Vaselli, O., and Török, K. (2002). Significance of silicate melt pockets in upper mantle xenoliths from the bakony–balaton Highland volcanic field, western Hungary. *Lithos* 61 (1-2), 79–102. doi:10.1016/S0024-4937(01)00075-5

Bali, E., Falus, Gy., Szabó, C., Peate, D. W., Hidas, K., Török, K., et al. (2007). Remnants of boninitic melts in the upper mantle beneath the central Pannonian Basin? *Mineral. Petrol.* 90 (1), 51–72. doi:10.1007/s00710-006-0167-z

Bali, E., Zajacz, Z., Kovacs, I., Szabó, C., Halter, W., Vaselli, O., et al. (2008). A quartz-bearing orthopyroxene-rich websterite xenolith from the Pannonian Basin, western Hungary: Evidence for release of quartz-saturated melts from a subducted slab. *J. Petrol.* 49 (3), 421–439. doi:10.1093/petrology/egm086

Bali, E., Hidas, K., Guðfinnsson, G. H., Kovács, Z., Török, K., and Román-Alpiste, M. J. (2018). Zircon and apatite-bearing pyroxene hornblendite mantle xenolith from Hungary, Carpathian-Pannonian region. *Lithos* 316, 19–32. doi:10.1016/j.lithos.2018.07.004

Balogh, K., and Németh, K. (2005). Evidence for the neogene small-volume intracontinental volcanism in Western Hungary: K/Ar geochronology of the Tihany maar volcanic complex. *Geol. Carpathica* 56 (1), 91–99.

Bebout, G. E. (2007). Metamorphic chemical geodynamics of subduction zones. *Earth Planet. Sci. Lett.* 260 (3-4), 373–393. doi:10.1016/j.epsl.2007.05.050

Bénard, A., Le Losq, C., Müntener, O., Robyr, M., Nebel, O., Arculus, R. J., et al. (2022). Spinel harzburgite-derived silicate melts forming sulfide-bearing orthopyroxenite in the lithosphere. Part 1: partition coefficients and volatile evolution accompanying fluid- and redox-induced sulfide formation. *Front. Earth Sci. (Lausanne).* 10, 867979. doi:10.3389/feart.2022.867979

Benedek, K., Pécskay, Z., Szabó, C., Jósvai, J., and Németh, T. (2004). Paleogene igneous rocks in the zala basin (Western Hungary): Link to the Paleogene magmatic activity along the periadriatic lineament. *Geol. Carpathica* 55 (1), 43–50.

Berkesi, M., Guzmics, T., Szabó, C., Dubessy, J., Bodnar, R. J., Hidas, K., et al. (2012). The role of CO_2-rich fluids in trace element transport and metasomatism in the lithospheric mantle beneath the Central Pannonian Basin, Hungary, based on fluid inclusions in mantle xenoliths. *Earth Planet. Sci. Lett.* 331, 8–20. doi:10.1016/j.epsl.2012.03.012

Brey, G. P., and Köhler, T. (1990). Geothermobarometry in four-phase lherzolites II. New thermobarometers, and practical assessment of existing thermobarometers. *J. Petrol.* 31 (6), 1353–1378. doi:10.1093/petrology/31.6.1353

Chauvel, C., Goldstein, S. L., and Hofmann, A. W. (1995). Hydration and dehydration of oceanic crust controls Pb evolution in the mantle. *Chem. Geol.* 126 (1), 65–75. doi:10.1016/0009-2541(95)00103-3

Chen, L. H., and Zhou, X. H. (2005). Subduction-related metasomatism in the thinning lithosphere: Evidence from a composite dunite-orthopyroxenite xenolith entrained in Mesozoic Laiwu high-Mg diorite, North China Craton. *Geochem. Geophys. Geosyst.* 6 (6), 1–20. doi:10.1029/2005GC000938

Coltorti, M., Bonadiman, C., Faccini, B., Grégoire, M., O'Reilly, S. Y., and Powell, W. (2007). Amphiboles from suprasubduction and intraplate lithospheric mantle. *Lithos* 99 (1-2), 68–84. doi:10.1016/j.lithos.2007.05.009

Créon, L., Rouchon, V., Youssef, S., Rosenberg, E., Delpech, G., Szabo, Cs., et al. (2017a). Highly CO_2-supersaturated melts in the Pannonian lithospheric mantle–A transient carbon reservoir? *Lithos* 286, 519–533. doi:10.1016/j.lithos.2016.12.009

Créon, L., Delpech, G., Rouchon, V., and Guyot, F. (2017b). Slab-derived metasomatism in the Carpathian-Pannonian mantle revealed by investigations of mantle xenoliths from the Bakony-Balaton Highland Volcanic Field. *Lithos* 286, 534–552. doi:10.1016/j.lithos.2017.06.004

Csontos, L., and Nagymarosy, A. (1998). The mid-Hungarian line: a zone of repeated tectonic inversions. *Tectonophysics* 297 (1-4), 51–71. doi:10.1016/S0040-1951(98)00163-2

Csontos, L., and Vörös, A. (2004). Mesozoic plate tectonic reconstruction of the Carpathian region. *Palaeogeogr. Palaeoclimatol. Palaeoecol.* 210 (1), 1–56. doi:10.1016/j.palaeo.2004.02.033

Csontos, L. (1995). Tertiary tectonic evolution of the intra-carpathian area: a review. *Acta Vulcanol.* 7 (2), 1–13.

Dai, H. K., and Zheng, J. P. (2019). Mantle xenoliths and host basalts record the Paleo-Asian oceanic materials in the mantle wedge beneath northwest North China Craton. *Solid Earth Sci.* 4 (4), 150–158. doi:10.1016/j.sesci.2019.09.001

Dantas, C., Grégoire, M., Koester, E., Conceição, R. V., and Rieck, N., Jr (2009). The lherzolite–websterite xenolith suite from northern patagonia (Argentina): Evidence of mantle–melt reaction processes. *Lithos* 107 (1-2), 107–120. doi:10.1016/j.lithos.2008.06.012

Dawson, J. B. (1984). Contrasting types of upper-mantle metasomatism? *Dev. Petrol.* 11 (2), 289–294. Elsevier. doi:10.1016/B978-0-444-42274-3.50030-5

Demény, A., Vennemann, T. W., Hegner, E., Nagy, G., Milton, J. A., Embey-Isztin, A., et al. (2004). Trace element and C–O–Sr–Nd isotope evidence for subduction-related carbonate–silicate melts in mantle xenoliths (Pannonian Basin, Hungary). *Lithos* 75 (1-2), 89–113. doi:10.1016/j.lithos.2003.12.016

Dick, H. J., Fisher, R. L., and Bryan, W. B. (1984). Mineralogic variability of the uppermost mantle along mid-ocean ridges. *Earth Planet. Sci. Lett.* 69 (1), 88–106. doi:10.1016/0012-821X(84)90076-1

Dobosi, G., Downes, H., Embey-Isztin, A., and Jenner, G. A. (2003). Origin of megacrysts and pyroxenite xenoliths from the Pliocene alkali basalts of the Pannonian Basin (Hungary). *Njma.* 178, 217–237. doi:10.1127/0077-7757/2003/0178-0217

Dobosi, G., Jenner, G. A., Embey-Isztin, A., and Downes, H. (2010). Cryptic metasomatism in clino-and orthopyroxene in the upper mantle beneath the Pannonian region. *Geol. Soc. Lond. Spec. Publ.* 337 (1), 177–194. doi:10.1144/SP337.9

Downes, H., Embey-Isztin, A., and Thirlwall, M. F. (1992). Petrology and geochemistry of spinel peridotite xenoliths from the Western Pannonian Basin (Hungary): Evidence for an association between enrichment and texture in the upper mantle. *Contr. Mineral. Petrol.* 109 (3), 340–354. doi:10.1007/BF00283323

Downes, H., Macdonald, R., Upton, B. G., Cox, K. G., Bodinierm, J. L., Mason, P. R. D., et al. (2004). Ultramafic xenoliths from the bearpaw Mountains, Montana, USA: Evidence for multiple metasomatic events in the lithospheric mantle beneath the Wyoming craton. *J. Petrol.* 45 (8), 1631–1662. doi:10.1093/petrology/egh027

Downes, H. (1997). "Shallow continental lithospheric mantle heterogeneity—petrological constraints," in *Upper mantle heterogeneities from active and passive seismology.* Editor K. Fuchs (Springer), 295–308. doi:10.1007/978-94-015-8979-6_29

Embey-Isztin, A., Scharbert, H. G., Dietrich, H., and Poultidis, H. (1989). Petrology and geochemistry of peridotite xenoliths in alkali basalts from the Transdanubian Volcanic Region, West Hungary. *J. Petrol.* 30 (1), 79–105. doi:10.1093/petrology/30.1.79

Embey-Isztin, A., Downes, H., James, D. E., Upton, B. G. J., Dobosi, G., Ingram, G. A., et al. (1993). The petrogenesis of pliocene alkaline volcanic rocks from the Pannonian Basin, eastern central Europe. *J. Petrol.* 34 (2), 317–343. doi:10.1093/petrology/34.2.317

Embey-Isztin, A., Dobosi, G., Altherr, R., and Meyer, H. P. (2001). Thermal evolution of the lithosphere beneath the Western Pannonian Basin: Evidence from deep-seated xenoliths. *Tectonophysics* 331 (3), 285–306. doi:10.1016/S0040-1951(00)00287-0

Embey-Isztin, A., Dobosi, G., Bodinier, J. L., Bosch, D., Jenner, G. A., Pourtales, S., et al. (2014). Origin and significance of poikilitic and mosaic peridotite xenoliths in the Western Pannonian Basin: geochemical and petrological evidences. *Contrib. Mineral. Petrol.* 168 (3), 1054–1116. doi:10.1007/s00410-014-1054-y

Embey-Isztin, A. (1976). Amphibolite/lherzolite composite xenolith from Szigliget, north of the Lake Balaton, Hungary. *Earth Planet. Sci. Lett.* 31, 297–304. doi:10.1016/0012-821X(76)90223-5

Ertan, I. E., and Leeman, W. P. (1996). Metasomatism of cascades subarc mantle: Evidence from a rare phlogopite orthopyroxenite xenolith. *Geology* 24 (5), 451–454. doi:10.1130/0091-7613(1996)024<0451:MOCSME>2.3.CO;2

Falus, Gy., Szabó, C., and Vaselli, O. (2000). Mantle upwelling within the Pannonian Basin: Evidence from xenolith lithology and mineral chemistry. *Terra nova.* 12 (6), 295–302. doi:10.1046/j.1365-3121.2000.00313.x

Falus, Gy., Drury, M. R., van Roermund, H. L., and Szabó, C. (2004). Magmatism-related localized deformation in the mantle: a case study. *Contrib. Mineral. Petrol.* 146 (4), 493–505. doi:10.1007/s00410-003-0513-7

Fodor, L., Csontos, L., Bada, G., Győrfi, I., and Benkovics, L. (1999). Tertiary tectonic evolution of the Pannonian Basin system and neighbouring orogens: a new synthesis of palaeostress data. *Geol. Soc. Lond. Spec. Publ.* 156 (1), 295–334. doi:10.1144/GSL.SP.1999.156.01.15

Garrido, C. J., and Bodinier, J. L. (1999). Diversity of mafic rocks in the ronda peridotite: Evidence for pervasive melt–rock reaction during heating of subcontinental lithosphere by upwelling asthenosphere. *J. Petrol.* 40 (5), 729–754. doi:10.1093/petroj/40.5.729

Gaul, O. F., Griffin, W. L., O'Reilly, S. Y., and Pearson, N. J. (2000). Mapping olivine composition in the lithospheric mantle. *Earth Planet. Sci. Lett.* 182 (3-4), 223–235. doi:10.1016/S0012-821X(00)00243-0

Green, D. H., and Ringwood, A. E. (1967). The genesis of basaltic magmas. *Contr. Mineral. Petrol.* 15 (2), 103–190. doi:10.1007/BF00372052

Grégoire, M., McInnes, B. I., and O'Reilly, S. Y. (2001). Hydrous metasomatism of oceanic sub-arc mantle, lihir, Papua New Guinea: Part 2. Trace element characteristics of slab-derived fluids. *Lithos* 59 (3), 91–108. doi:10.1016/S0024-4937(01)00058-5

Griffin, W. L., and O'Reilly, S. Y. (2007). Cratonic lithospheric mantle: is anything subducted? *Episodes* 30 (1), 43–53. doi:10.18814/epiiugs/2007/v30i1/006

Grove, T. L., Chatterjee, N., Parman, S. W., and Médard, E. (2006). The influence of H₂O on mantle wedge melting. *Earth Planet. Sci. Lett.* 249 (1-2), 74–89. doi:10.1016/j.epsl.2006.06.043

Hauri, E. H., Wagner, T. P., and Grove, T. L. (1994). Experimental and natural partitioning of Th, U, Pb and other trace elements between garnet, clinopyroxene and basaltic melts. *Chem. Geol.* 117 (1-4), 149–166. doi:10.1016/0009-2541(94)90126-0

Hawthorne, F. C., Oberti, R., Harlow, G. E., Maresch, W. V., Martin, R. F., Schumacher, J. C., et al. (2012). Nomenclature of the amphibole supergroup. *Am. Mineral.* 97 (11-12), 2031–2048. doi:10.2138/am.2012.4276

Hazra, A., Saha, A., Verencar, A., Satyanarayanan, M., Ganguly, S., Kotha, M., et al. (2021). Refertilization of mantle peridotites from the Central Indian Ridge: Response to a geodynamic transition. *Lithosphere* 2021 (6), 1–17. doi:10.2113/2021/9706924

Hermann, J., Spandler, C., Hack, A., and Korsakov, A. V. (2006). Aqueous fluids and hydrous melts in high-pressure and ultra-high pressure rocks: Implications for element transfer in subduction zones. *Lithos* 92 (3-4), 399–417. doi:10.1016/j.lithos.2006.03.055

Hidas, K., Falus, Gy., Szabó, C., Szabó, P. J., Kovács, I., and Földes, T. (2007). Geodynamic implications of flattened tabular equigranular textured peridotites from the Bakony-Balaton Highland Volcanic Field (Western Hungary). *J. Geodyn.* 43 (4-5), 484–503. doi:10.1016/j.jog.2006.10.007

Hidas, K., Guzmics, T., Szabó, C., Kovács, I., Bodnar, R. J., Zajacz, Z., et al. (2010). Coexisting silicate melt inclusions and H₂O-bearing, CO₂-rich fluid inclusions in mantle peridotite xenoliths from the Carpathian–Pannonian region (central Hungary). *Chem. Geol.* 274 (1-2), 1–18. doi:10.1016/j.chemgeo.2010.03.004

Hirschmann, M. M., Ghiorso, M. S., Wasylenki, L. E., Asimow, P. D., and Stolper, E. M. (1998). Calculation of peridotite partial melting from thermodynamic models of minerals and melts. I. Review of methods and comparison with experiments. *J. Petrol.* 39 (6), 1091–1115. doi:10.1093/petroj/39.6.1091

Horváth, F., and Cloetingh, S. A. P. L. (1996). Stress-induced late-stage subsidence anomalies in the Pannonian basin. *Tectonophysics* 266 (1-4), 287–300. doi:10.1016/S0040-1951(96)00194-1

Horváth, F. (1993). Towards a mechanical model for the formation of the Pannonian basin. *Tectonophysics* 226 (1-4), 333–357. doi:10.1016/0040-1951(93)90126-5

Houseman, G. A., and Gemmer, L. (2007). Intra-orogenic extension driven by gravitational instability: Carpathian-Pannonian orogeny. *Geol.* 35 (12), 1135–1138. doi:10.1130/G23993A.1

Ionov, D. A., Bodinier, J. L., Mukasa, S. B., and Zanetti, A. (2002). Mechanisms and sources of mantle metasomatism: major and trace element compositions of peridotite xenoliths from spitsbergen in the context of numerical modelling. *J. Petrol.* 43 (12), 2219–2259. doi:10.1093/petrology/43.12.2219

Ishimaru, S., Arai, S., Ishida, Y., Shirasaka, M., and Okrugin, V. M. (2007). Melting and multi-stage metasomatism in the mantle wedge beneath a frontal arc inferred from highly depleted peridotite xenoliths from the Avacha volcano, southern Kamchatka. *J. Petrol.* 48 (2), 395–433. doi:10.1093/petrology/egl065

Iwamori, H. (1998). Transportation of H₂O and melting in subduction zones. *Earth Planet. Sci. Lett.* 160 (1-2), 65–80. doi:10.1016/S0012-821X(98)00080-6

Jankovics, M. É., Sági, T., Astbury, R. L., Petrelli, M., Kiss, B., Ubide, T., et al. (2019). Olivine major and trace element compositions coupled with spinel chemistry to unravel the magmatic systems feeding monogenetic basaltic volcanoes. *J. Volcanol. Geotherm. Res.* 369, 203–223. doi:10.1016/j.jvolgeores.2018.11.027

Jochum, K. P., Willbold, M., Raczek, I., Stoll, B., and Herwig, K. (2005). Chemical characterisation of the USGS reference glasses GSA-1G, GSC-1G, GSD-1G, GSE-1G, BCR-2G, BHVO-2G and BIR-1G using EPMA, ID-TIMS, ID-ICP-MS and LA-ICP-MS. *Geostand. Geoanal. Res.* 29 (3), 285–302. doi:10.1111/j.1751-908X.2005.tb00901.x

Johan, Z., Martin, R. F., and Ettler, V. (2017). Fluids are bound to be involved in the formation of ophiolitic chromite deposits. *Eur. J. Mineral.* 29 (4), 543–555. doi:10.1127/ejm/2017/0029-2648

Kázmér, M., and Kovács, S. (1985). Permian-paleogene paleogeography along the eastern part of the insubric-periadriatic lineament system: Evidence for continental escape of the bakony-drauzug unit. *Acta Geol. Hung.* 28 (1-2), 71–84.

Kelemen, P. B., Dick, H. J., and Quick, J. E. (1992). Formation of harzburgite by pervasive melt/rock reaction in the upper mantle. *Nature* 358 (6388), 635–641. doi:10.1038/358635a0

Kelemen, P. B., Shimizu, N., and Salters, V. J. (1995). Extraction of mid-ocean-ridge basalt from the upwelling mantle by focused flow of melt in dunite channels. *Nature* 375 (6534), 747–753. doi:10.1038/375747a0

Kelemen, P. B., Hart, S. R., and Bernstein, S. (1998). Silica enrichment in the continental upper mantle via melt/rock reaction. *Earth Planet. Sci. Lett.* 164 (1-2), 387–406. doi:10.1016/S0012-821X(98)00233-7

Kelemen, P. B. (1990). Reaction between ultramafic rock and fractionating basaltic magma I. Phase relations, the origin of calc-alkaline magma series, and the formation of discordant dunite. *J. Petrol.* 31 (1), 51–98. doi:10.1093/petrology/31.1.51

Keppler, H. (1996). Constraints from partitioning experiments on the composition of subduction-zone fluids. *Nature* 380 (6571), 237–240. doi:10.1038/380237a0

Keresztúri, G., and Németh, K. (2011). Shallow-seated controls on the evolution of the upper pliocene kopasz-hegy nested monogenetic volcanic chain in the western Pannonian Basin (Hungary). *Geol. Carpath.* 62 (6), 535–546. doi:10.2478/v10096-011-0038-3

Kessel, R., Schmidt, M. W., Ulmer, P., and Pettke, T. (2005). Trace element signature of subduction-zone fluids, melts and supercritical liquids at 120–180 km depth. *Nature* 437 (7059), 724–727. doi:10.1038/nature03971

Kovács, I., and Szabó, C. (2008). Middle Miocene volcanism in the vicinity of the middle Hungarian zone: Evidence for an inherited enriched mantle source. *J. Geodyn.* 45 (1), 1–17. doi:10.1016/j.jog.2007.06.002

Kovács, I., Csontos, L., Szabó, C., Bali, E., Falus, Gy., Benedek, K., et al. (2007). Paleogene-early Miocene igneous rocks and geodynamics of the alpine-carpathian-pannonian-dinaric region: an integrated approach. *Geol. Soc. Am. - Special Pap.* 418, 93–112. doi:10.1130/2007.2418(05

Kovács, I., Patkó, L., Liptai, N., Lange, T. P., Taracsák, Z., Cloetingh, S. A. P. L., et al. (2020). The role of water and compression in the genesis of alkaline basalts: Inferences from the Carpathian-Pannonian region. *Lithos* 354, 105323. doi:10.1016/j.lithos.2019.105323

Le Roux, V., Bodinier, J. L., Tommasi, A., Alard, O., Dautria, J. M., Vauchez, A., et al. (2007). The lherz spinel lherzolite: refertilized rather than pristine mantle. *Earth Planet. Sci. Lett.* 259 (3-4), 599–612. doi:10.1016/j.epsl.2007.05.026

Le Roux, V., Dick, H. J. B., and Shimizu, N. (2014). Tracking flux melting and melt percolation in supra-subduction peridotites (Josephine ophiolite, USA). *Contrib. Mineral. Petrol.* 168 (4), 1064–1122. doi:10.1007/s00410-014-1064-9

Lenoir, X., Garrido, C. J., Bodinier, J. L., and Dautria, J. M. (2000). Contrasting lithospheric mantle domains beneath the Massif Central (France) revealed by geochemistry of peridotite xenoliths. *Earth Planet. Sci. Lett.* 181 (3), 359–375. doi:10.1016/S0012-821X(00)00216-8

Liang, Y., Sun, C., and Yao, L. (2013). A REE-in-two-pyroxene thermometer for mafic and ultramafic rocks. *Geochim. Cosmochim. Acta* 102, 246–260. doi:10.1016/j.gca.2012.10.035

Liptai, N., Patkó, L., Kovács, I. J., Hidas, K., Pintér, Zs., Jeffries, T., et al. (2017). Multiple metasomatism beneath the Nógrád–Gömör Volcanic Field (Northern

Pannonian Basin) revealed by upper mantle peridotite xenoliths. *J. Petrol.* 58 (6), 1107–1144. doi:10.1093/petrology/egx048

Liptai, N., Lange, T. P., Patkó, L., Pintér, Zs., Berkesi, M., Aradi, L. E., et al. (2021). Effect of water on the rheology of the lithospheric mantle in young extensional basin systems as shown by xenoliths from the Carpathian-Pannonian region. *Glob. Planet. Change* 196, 103364. doi:10.1016/j.gloplacha.2020.103364

Malaspina, N., Hermann, J., Scambelluri, M., and Compagnoni, R. (2006). Polyphase inclusions in garnet–orthopyroxenite (Dabie Shan, China) as monitors for metasomatism and fluid-related trace element transfer in subduction zone peridotite. *Earth Planet. Sci. Lett.* 249 (3-4), 173–187. doi:10.1016/j.epsl.2006.07.017

Mallik, A., and Dasgupta, R. (2012). Reaction between MORB-eclogite derived melts and fertile peridotite and generation of ocean island basalts. *Earth Planet. Sci. Lett.* 329, 97–108. doi:10.1016/j.epsl.2012.02.007

Manning, C. E. (2004). The chemistry of subduction-zone fluids. *Earth Planet. Sci. Lett.* 223 (1-2), 1–16. doi:10.1016/j.epsl.2004.04.030

McDonough, W. F., and Sun, S. S. (1995). The composition of the Earth. *Chem. Geol.* 120 (3-4), 223–253. doi:10.1016/0009-2541(94)00140-4

McInnes, B. I., Gregoire, M., Binns, R. A., Herzig, P. M., and Hannington, M. D. (2001). Hydrous metasomatism of oceanic sub-arc mantle, lihir, Papua New Guinea: petrology and geochemistry of fluid-metasomatised mantle wedge xenoliths. *Earth Planet. Sci. Lett.* 188 (1-2), 169–183. doi:10.1016/S0012-821X(01)00306-5

Mercier, J. C., and Nicolas, A. (1975). Textures and fabrics of upper-mantle peridotites as illustrated by xenoliths from basalts. *J. Petrol.* 16 (1), 454–487. doi:10.1093/petrology/16.1.454

Miller, D. M., Goldstein, S. L., and Langmuir, C. H. (1994). Cerium/lead and lead isotope ratios in arc magmas and the enrichment of lead in the continents. *Nature* 368 (6471), 514–520. doi:10.1038/368514a0

Morgan, Z., and Liang, Y. (2005). An experimental study of the kinetics of lherzolite reactive dissolution with applications to melt channel formation. *Contrib. Mineral. Petrol.* 150 (4), 369–385. doi:10.1007/s00410-005-0033-8

Navon, O., and Stolper, E. (1987). Geochemical consequences of melt percolation: the upper mantle as a chromatographic column. *J. Geol.* 95 (3), 285–307. doi:10.1086/629131

Nédli, Zs., Princivalle, F., Dobosi, G., and Embey-Isztin, A. (2009). Crystal chemistry of clinopyroxenes from upper-mantle xenolith series in the Balaton–Bakony volcanic area (Carpathian–Pannonian region, Hungary). *Eur. J. Mineral.* 21 (2), 433–442. doi:10.1127/0935-1221/2009/0021-1906

Németh, K., and Martin, U. (1999). Large hydrovolcanic field in the Pannonian Basin: general characteristics of the bakony-balaton Highland volcanic field, Hungary. *Acta Vulcanol.* 11 (2), 271–282.

Németh, B., Török, K., Bali, E., Zajacz, Z., Fodor, L., and Szabó, C. (2021). Melt-rock interaction in the lower crust based on silicate melt inclusions in mafic garnet granulite xenoliths, Bakony-Balaton Highland. *Geol. Carpath.* 72 (3), 232–252. doi:10.31577/GeolCarp.72.3.4

Nimis, P., and Grütter, H. (2010). Internally consistent geothermometers for garnet peridotites and pyroxenites. *Contrib. Mineral. Petrol.* 159 (3), 411–427. doi:10.1007/s00410-009-0455-9

Niu, Y. (1997). Mantle melting and melt extraction processes beneath ocean ridges: evidence from abyssal peridotites. *J. Petrol.* 38 (8), 1047–1074. doi:10.1093/petroj/38.8.1047

Niu, Y. (2004). Bulk-rock major and trace element compositions of abyssal peridotites: implications for mantle melting, melt extraction and post-melting processes beneath mid-ocean ridges. *J. Petrol.* 45 (12), 2423–2458. doi:10.1093/petrology/egh068

Ntaflos, T., Bizimis, M., and Abart, R. (2017). Mantle xenoliths from Szentbékálla, Balaton: Geochemical and petrological constraints on the evolution of the lithospheric mantle underneath Pannonian Basin, Hungary. *Lithos* 276, 30–44. doi:10.1016/j.lithos.2016.12.018

O'Reilly, S. Y., and Griffin, W. L. (2013). "Mantle metasomatism," in *Metasomatism and the chemical transformation of rock* (Berlin, Heidelberg: Springer), 471–533. doi:10.1007/978-3-642-28394-9_12

Parkinson, I. J., and Pearce, J. A. (1998). Peridotites from the izu–bonin–mariana forearc (ODP leg 125): Evidence for mantle melting and melt–mantle interaction in a supra-subduction zone setting. *J. Petrol.* 39 (9), 1577–1618. doi:10.1093/petroj/39.9.1577

Patkó, L., Liptai, N., Aradi, L. E., Klébesz, R., Sendula, E., Bodnar, R. J., et al. (2020). Metasomatism-induced wehrlite formation in the upper mantle beneath the nógrád-gömör volcanic field (northern Pannonian Basin): evidence from xenoliths. *Geosci. Front.* 11 (3), 943–964. doi:10.1016/j.gsf.2019.09.012

Paton, C., Hellstrom, J., Paul, B., Woodhead, J., and Hergt, J. (2011). Iolite: Freeware for the visualisation and processing of mass spectrometric data. *J. Anal. At. Spectrom.* 26 (12), 2508–2518. doi:10.1039/c1ja10172b

Pearce, N. J., Perkins, W. T., Westgate, J. A., Gorton, M. P., Jackson, S. E., Neal, C. R., et al. (1997). A compilation of new and published major and trace element data for NIST SRM 610 and NIST SRM 612 glass reference materials. *Geostand. Geoanal. Res.* 21 (1), 115–144. doi:10.1111/j.1751-908X.1997.tb00538.x

Pécskay, Z., Lexa, J., Szakács, A., Seghedi, I., Balogh, K., Konečný, V., et al. (2006). Geochronology of Neogene magmatism in the Carpathian arc and intra-Carpathian area. *Geol. Carpathica* 57 (6), 511.

Perinelli, C., Gaeta, M., and Armienti, P. (2017). Cumulate xenoliths from Mt. Overlord, northern victoria land, Antarctica: A window into high pressure storage and differentiation of mantle-derived basalts. *Lithos* 268-271, 225–239. doi:10.1016/j.lithos.2016.10.027

Pike, J. E. N., and Schwarzman, E. C. (1977). Classification of textures in ultramafic xenoliths. *J. Geol.* 85, 49–61. doi:10.1086/628268

Pouchou, J. L., and Pichoir, F. (1991). "Quantitative analysis of homogeneous or stratified microvolumes applying the model "PAP"," in *Electron probe quantitation*. Editors K. F. J. Heinrich and D. E. Newbury (Boston, MA: Springer). doi:10.1007/978-1-4899-2617-3_4

Puziewicz, J., Matusiak-Małek, M., Ntaflos, T., Grégoire, M., and Kukuła, A. (2015). Subcontinental lithospheric mantle beneath central Europe. *Int. J. Earth Sci.* 104 (8), 1913–1924. doi:10.1007/s00531-014-1134-2

Ratschbacher, L., Frisch, W., Linzer, H. G., and Merle, O. (1991). Lateral extrusion in the eastern alps, part 2: structural analysis. *Tectonics* 10 (2), 257–271. doi:10.1029/90TC02623

Regelous, M., Gamble, J. A., and Turner, S. P. (2010). Mechanism and timing of Pb transport from subducted oceanic crust and sediment to the mantle source of arc lavas. *Chem. Geol.* 273 (1-2), 46–54. doi:10.1016/j.chemgeo.2010.02.011

Roduit, N. (2006). *MicroVision: Image analysis toolbox for measuring and quantifying components of high-definition images*. Version 1.2.2. Available at: http://www.jmicrovision.com (Accessed July 02, 2006).

Royden, L. H., Horvath, F., and Burchfiel, B. C. (1982). Transform faulting, extension, and subduction in the Carpathian Pannonian region. *Geol. Soc. Am. Bull.* 93 (8), 717–725. doi:10.1130/0016-7606(1982)93<717:TFEASI>2.0.CO;2

Rudnick, R. L., McDonough, W. F., and Chappell, B. W. (1993). Carbonatite metasomatism in the northern Tanzanian mantle: petrographic and geochemical characteristics. *Earth Planet. Sci. Lett.* 114 (4), 463–475. doi:10.1016/0012-821X(93)90076-L

Saha, A., Basu, A. R., Jacobsen, S. B., Poreda, R. J., Yin, Q. Z., and Yogodzinski, G. M. (2005). Slab devolatilization and Os and Pb mobility in the mantle wedge of the Kamchatka arc. *Earth Planet. Sci. Lett.* 236 (1-2), 182–194. doi:10.1016/j.epsl.2005.05.018

Seghedi, I., and Downes, H. (2011). Geochemistry and tectonic development of Cenozoic magmatism in the Carpathian–Pannonian region. *Gondwana Res.* 20 (4), 655–672. doi:10.1016/j.gr.2011.06.009

Seghedi, I., Downes, H., Vaselli, O., Szakács, A., Balogh, K., and Pécskay, Z. (2004). Post-collisional tertiary–quaternary mafic alkalic magmatism in the carpathian–pannonian region: a review. *Tectonophysics* 393 (1-4), 43–62. doi:10.1016/j.tecto.2004.07.051

Shaw, C. S., Lebert, B. S., and Woodland, A. B. (2018). Thermodynamic modelling of mantle–melt interaction evidenced by veined Wehrlite xenoliths from the Rockeskyllerkopf volcanic complex, west Eifel volcanic field, Germany. *J. Petrol.* 59 (1), 59–86. doi:10.1093/petrology/egy018

Smith, D., Riter, J. A., and Mertzman, S. A. (1999). Water–rock interactions, orthopyroxene growth, and Si-enrichment in the mantle: Evidence in xenoliths from the Colorado plateau, southwestern United States. *Earth Planet. Sci. Lett.* 165 (1), 45–54. doi:10.1016/S0012-821X(98)00251-9

Spandler, C., and O'Neill, H. S. C. (2010). Diffusion and partition coefficients of minor and trace elements in San Carlos olivine at 1, 300 C with some geochemical implications. *Contrib. Mineral. Petrol.* 159 (6), 791–818. doi:10.1007/s00410-009-0456-8

Staudigel, H. (2003). Hydrothermal alteration processes in the oceanic crust. *Treatise Geochem.* 3, 511–535. doi:10.1016/B0-08-043751-6/03032-2

Stegena, L., Géczy, B., and Horváth, F. (1975). Late cenozoic evolution of the Pannonian basin. *Tectonophysics* 26 (1-2), 71–90. doi:10.1016/0040-1951(75)90114-6

Streckeisen, A. (1976). To each plutonic rock its proper name. *Earth-Sci. Rev.* 12 (1), 1–33. doi:10.1016/0012-8252(76)90052-0

Szabó, C., Harangi, Sz., and Csontos, L. (1992). Review of neogene and quaternary volcanism of the carpathian-pannonian region. *Tectonophysics* 208 (1-3), 243–256. doi:10.1016/0040-1951(92)90347-9

Szabó, C., Vaselli, O., Vannucci, R., Bottazzi, P., Ottolini, L., Coradossi, N., et al. (1995). Ultramafic xenoliths from the Little Hungarian plain (western Hungary): a petrologic and geochemical study. *Acta Vulcanol.* 7, 249–264.

Szabó, C., Falus, Gy., Zajacz, Z., Kovács, I., and Bali, E. (2004). Composition and evolution of lithosphere beneath the carpathian–pannonian region: a review. *Tectonophysics* 393 (1-4), 119–137. doi:10.1016/j.tecto.2004.07.031

Szabó, C., Hidas, K., Bali, E., Zajacz, Z., Kovács, I., Yang, K., et al. (2009). Melt–wall rock interaction in the mantle shown by silicate melt inclusions in peridotite xenoliths from the central Pannonian Basin (Western Hungary). *Isl. Arc* 18 (2), 375–400. doi:10.1111/j.1440-1738.2009.00672.x

Tamura, A., and Arai, S. (2006). Harzburgite–dunite–orthopyroxenite suite as a record of supra-subduction zone setting for the Oman ophiolite mantle. *Lithos* 90 (1-2), 43–56. doi:10.1016/j.lithos.2005.12.012

Tenthorey, E., and Hermann, J. (2004). Composition of fluids during serpentinite breakdown in subduction zones: Evidence for limited boron mobility. *Geol.* 32 (10), 865–868. doi:10.1130/G20610.1

Török, K., and De Vivo, B. (1995). Fluid inclusions in upper mantle xenoliths from the Balaton Highland, Western Hungary. *Acta Vulcanol.* 7, 277–284.

Török, K., Németh, B., Koller, F., Dégi, J., Badenszki, E., Szabó, C., et al. (2014). Evolution of the middle crust beneath the Western Pannonian Basin: a xenolith study. *Mineral. Petrol.* 108 (1), 33–47. doi:10.1007/s00710-013-0287-1

Wang, J., Hattori, K. H., and Stern, C. R. (2008). Metasomatic origin of garnet orthopyroxenites in the subcontinental lithospheric mantle underlying Pali Aike volcanic field, southern South America. *Mineral. Petrol.* 94 (3), 243–258. doi:10.1007/s00710-008-0017-2

Wang, C., Liang, Y., Dygert, N., and Xu, W. (2016). formation of orthopyroxenite by reaction between peridotite and hydrous basaltic melt: an experimental study. *Contrib. Mineral. Petrol.* 171 (8), 77–18. doi:10.1007/s00410-016-1287-z

Wijbrans, J., Németh, K., Martin, U., and Balogh, K. (2007). 40Ar/39Ar geochronology of Neogene phreatomagmatic volcanism in the Western Pannonian Basin, Hungary. *J. Volcanol. Geotherm. Res.* 164 (4), 193–204. doi:10.1016/j.jvolgeores.2007.05.009

Witt-Eickschen, G., and Seck, H. A. (1991). Solubility of Ca and Al in orthopyroxene from spinel peridotite: an improved version of an empirical geothermometer. *Contr. Mineral. Petrol.* 106 (4), 431–439. doi:10.1007/BF00321986

Yaxley, G. M., Anenburg, M., Tappe, S., Decree, S., and Guzmics, T. (2022). Carbonatites: Classification, sources, evolution, and emplacement. *Annu. Rev. Earth Planet. Sci.* 50, 261–293. doi:10.1146/annurev-earth-032320-104243

Yoshikawa, M., Niida, K., and Green, D. H. (2018). Dunite channels within a harzburgite layer from the Horoman peridotite complex, Japan: Possible pathway for magmas. *Isl. Arc* 28 (1), e12279. doi:10.1111/iar.12279

Zheng, J., O'Reilly, S. Y., Griffin, W. L., Lu, F., Zhang, M., and Pearson, N. J. (2001). Relict refractory mantle beneath the eastern north China block: significance for lithosphere evolution. *Lithos* 57 (1), 43–66. doi:10.1016/S0024-4937(00)00073-6